Micellar Nanogels from Alginate-Based Diblock Copolysaccharides

Martin Fauquignon, Amalie Solberg, Lionel Porcar, Jean-Paul Chapel, Bjørn E Christensen, Christophe Schatz

Author version of article published in *Biomacromolecules* 2024, doi: 10.1021/acs.biomac.4c00717

Micellar Nanogels From Alginate-based Diblock Copolysaccharides

Martin Fauquignon,[a] *Amalie Solberg,*[b] *Lionel Porcar,*[c] *Jean-Paul Chapel,*[d] *Bjørn E. Christensen,*[b,*] *Christophe Schatz*[a,*]

[a]Université de Bordeaux, CNRS, Bordeaux INP, Laboratoire de chimie des polymères organiques (LCPO), UMR 5629, F-33600 Pessac, France

[b]NOBIPOL, Department of Biotechnology and Food Science, NTNU Norwegian University of Science and Technology, Sem Sælands vei 6/8, NO-7491 Trondheim, Norway

[c]Institut Laue-Langevin (ILL), F-38042, Grenoble, France

[d]Centre de Recherche Paul Pascal (CRPP), UMR CNRS 5031, Université de Bordeaux, F-33600 Pessac, France

Author version of article published in *Biomacromolecules* 2024, doi: 10.1021/acs.biomac.4c00717

ABSTRACT

Alginates are marine polysaccharides known for their ability to selectively bind calcium ions and form hydrogels. They are widely used in biomedical applications but are challenging to produce as nanogels. Here we introduce a self-assembly route to create stable alginate-based nanogels under near-equilibrium conditions. Guluronate (G) blocks, which interact with divalent cations such as Ca^{2+}, Ba^{2+}, and Sr^{2+}, were extracted from alginates and covalently linked through their reducing end to the reducing end of dextran (Dex) chains, forming linear block copolymers that self-assemble into micellar nanogels with a core-corona structure in the presence of these ions. Real-time DLS and SANS were used to study the self-assembly mechanism of the copolymer during dialysis against divalent ions. For the G_{12}-*b*-Dex_{51} copolymer, we achieved spherical micelles with an 8 nm radius and an aggregation number of around 20. Although the type of divalent cation affected micelle stability, it did not influence their size. Micellar nanogels are dynamic structures, capable of ion exchange, and can disassemble with chelating agents like EDTA.

KEYWORDS : alginate, block copolymer, self-assembly, dialysis, nanogel, micelle

Author version of article published in *Biomacromolecules* 2024, doi: 10.1021/acs.biomac.4c00717

INTRODUCTION

As a green and abundant resource, polysaccharides are on the rise not only for mass-market applications such as packaging but also for high value-added applications, notably biomedicine and biotechnology, owing to their remarkable diversity of physicochemical and biological properties.[1] Many polysaccharides are stimuli-responsive towards triggers such as pH, temperature, specific ions, or solvent exchange. Responses generally lead to conformational transitions which are often - but not always - associated with precipitation or gel formation. This is the case for alginates, which are well known for their propensity to form gel in aqueous solution when exposed to certain divalent ions such as calcium. Alginate hydrogels are primarily used as artificial extracellular matrix materials for tissue engineering, wound healing, cell encapsulation and drug delivery.[2,3]

Alginates comprise a family of polysaccharides isolated from brown seaweeds and some bacterial species.[4] They are unbranched chains containing residues of 1,4- linked β-D-mannuronate (M) and its C-5 epimer, 1,4-linked α-L-guluronate (G) (Figure 1). The distribution of M and G residues is neither regular nor random. Instead, alginates contain both M-blocks, G-blocks, and polyalternating MG-blocks. They can be isolated by partial hydrolysis combined with fractional precipitation (Figure 1).[5,6] The block-like structure results from a rather unusual biosynthesis where the homopolymer mannuronan is first synthesized, before guluronate residues are formed by processive enzymes (epimerases) in a post polymerization step (Figure 1). The G-blocks are responsible for Ca-induced chain-chain interactions and subsequent gelation of alginates.[7] The initial chain dimerization is generally described by the classical egg-box model (Figure 1).[8,9] Due to their $^{1}C_{4}$ conformation, G-blocks have (compared to M-and MG-blocks) a more contracted

conformation with higher charge density and cavities for Ca-coordination, leading to strong exothermic interactions between two or more G-blocks and Ca^{2+} ions.[10] The affinity and selectivity of G-blocks with some alkaline earth metals is shown to increase in the order of $Mg^{2+} << Ca^{2+} < Sr^{2+} < Ba^{2+}$.[5]

Alginate gelation has been extensively studied on small scales to produce microgel or nanogel particles for various applications, including drug delivery systems and imaging agents.[11–13] Traditional methods for designing nano-sized alginate systems focus on manipulating gelation parameters (reactant concentration, pH, additives, shear),[13,14] or by compartmentalizing the reaction volume using water-in-oil emulsion templates[15,16] or microfluidic methods.[17–19] However, these approaches typically do not produce particles that are in thermodynamic equilibrium. In such systems, the characteristics of the particles are influenced by the kinetics of the assembly process (i.e., how fast or slow the components meet, interact and form structures), leading to variability in particle size and structure. In contrast, under equilibrium conditions, the system reaches a stable state where the characteristics are determined solely by the thermodynamics (i.e., the composition and intrinsic properties of the components), regardless of the specific assembly route. Achieving equilibrium conditions is therefore essential to guarantee the consistency and reproducibility of nanogels, which is crucial when considering their large-scale production.

To obtain alginate-based nanogels that approach thermodynamic equilibrium, we propose a self-assembly strategy using double hydrophilic block copolymers (DHBCs).[20] These copolymers, typically composed of a polyacid and a neutral water-soluble polymer, are known to self-assemble into micellar structures through electrostatic interactions with multivalent metal cations, as recently reviewed.[21] The micelle characteristics are dependent on the block copolymer molar mass and composition. However, DHBCs made exclusively from polysaccharides have not been

explored, largely due to the difficulty of synthesizing them.[22,23] We have recently developed a simple, catalysis-free and cost-effective "click" chemistry approach that allows any pair of polysaccharides to be coupled at their reducing end using commercially available linkers based on alpha nucleophiles such as dihydrazides or, preferably, dioxyamines.[24–29] Here, the DBHCs synthesized consisted of a guluronate (G-block) and a dextran block (Figure 1).[6,28] By using G-blocks, we expect to enhance the affinity for divalent ions (such as calcium), surpassing both the parent alginates[28] and synthetic polyacids used in DHBCs.[30–34] Besides, dextran, a biodegradable bacterial exopolysaccharide, is an attractive alternative to polyethylene glycol (PEG) in drug delivery due to its biocompatibility and simple repeating glucose units.[35,36]

In this work, we investigate the self-assembly of oligoguluronate-*block*-dextran (G_m-*b*-Dex_n) copolysaccharides in the presence of Ca^{2+}, Sr^{2+}, and Ba^{2+} ions. The objective is to achieve nanogel structures based on a G core crosslinked by divalent ions, surrounded by a stabilizing dextran corona. We will refer them as micellar nanogels. Unlike traditional micelles formed by amphiphilic block copolymers, the gel-like core is expected to enhance the stability of the self-assembly. Achieving small, finite-size micellar nanogels (< 100 nm) requires precise stoichiometric control between the ions and G units, as well as strict phase separation between the dextran corona and the G-block core.[37] Under these conditions, the characteristics of the micellar nanogels should be fully governed by the molar mass and composition of the copolymer.

As stated previously, in a true equilibrium system, the mixing pathway should not influence the self-assembly properties. However, in practice it is well-known that block copolymer assemblies can be trapped in long-lived metastable states due to slow polymer chain dynamics associated with large molecular weights.[38–42] In order to favour the formation of micellar nanogels under near-equilibrium conditions, the copolymer solution will be dialyzed against a solution of divalent ions,

allowing for a slow and controlled self-assembly process. A dedicated dialysis cell will be employed to enable *in situ* monitoring of the nanogel formation by light and small-angle neutron scattering (Figure 1).[43] We will also compare this method with more conventional mixing techniques in order to assess the impact of the different assembly processes on the final nanogel properties.

The characteristics of the nanogels, including their stability under physiological conditions and disassembly in the presence of chelating agents, will be closely examined. Understanding how the composition of the block copolymers and the type of divalent ions influence the nanogels' physical properties is essential for assessing their potential in applications such as nanomedicine. Specifically, these micellar nanogels could serve as MRI contrast agents with heavy metal ions, offering advantages over other polysaccharide-based nanostructures due to their unique gel-like core and enhanced stability.

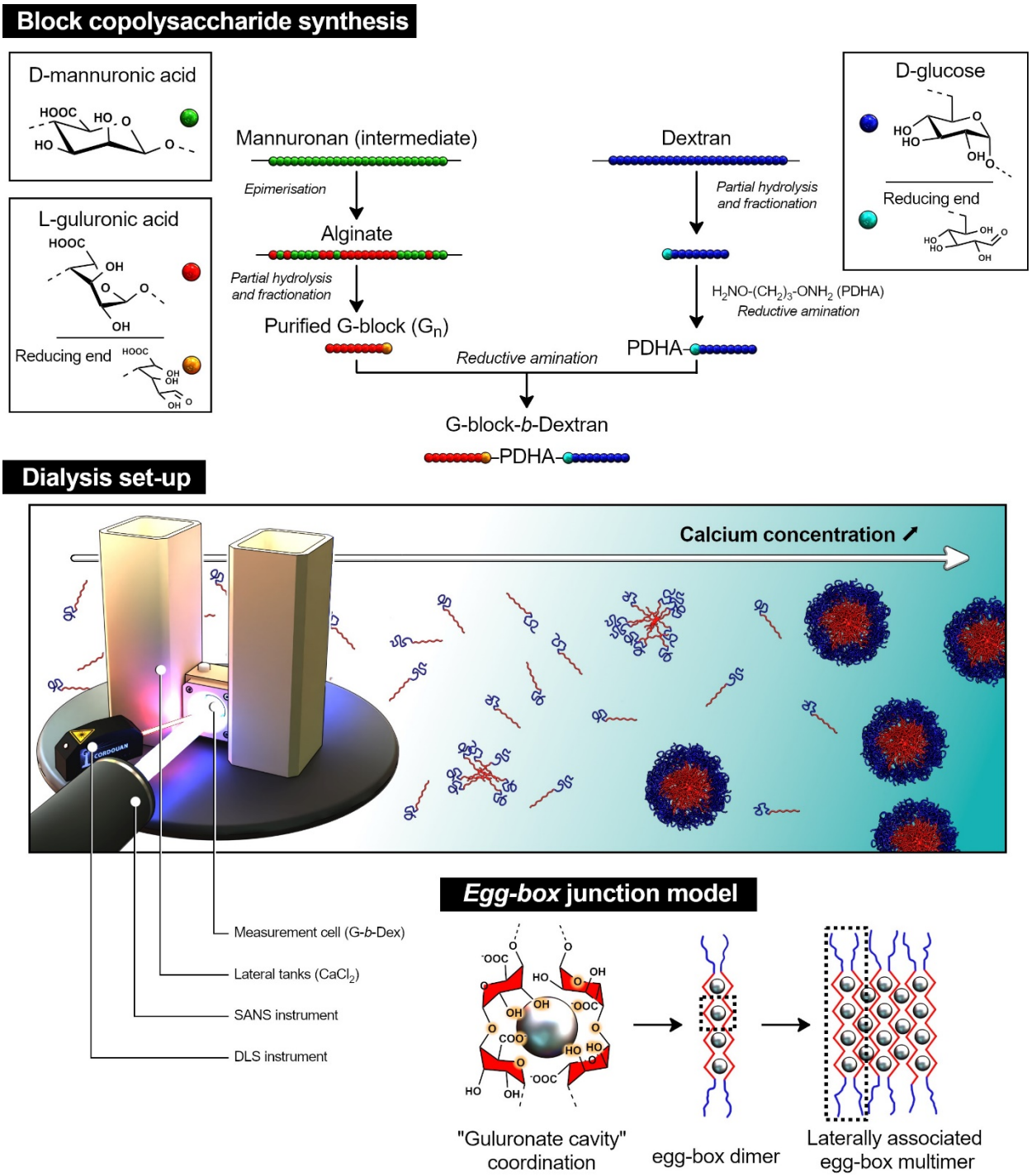

Figure 1. Rationale towards the synthesis and self-assembly of oligoguluronate-*b*-dextran (G_m-*b*-Dex_n) copolysaccharides into micellar nanogels through coordination of the G blocks with divalent ions (calcium here as an example). *Block copolysaccharide synthesis:* block-like structure of alginates originating from the epimerization of mannuronan. G blocks are excised through

selective acid precipitation of high guluronate alginate. (left) Partial acid hydrolysis and fractionation of dextran by GFC and the subsequent activation of the reducing end with PDHA. (right) Synthesis of G_m-*b*-Dex_n block copolysaccharide by end coupling of G_m and Dex_n-PDHA blocks. (bottom). *Dialysis setup:* home-made dialysis cell used for continuous kinetic monitoring of block copolysaccharide self-assembly in presence of divalent ions. A cellulose membrane of defined porosity is inserted between the central scattering cell containing the copolymer solution and the lateral reservoirs containing the $CaCl_2$ solution. The gradual diffusion of divalent ions triggers the stepwise formation of micellar nanogels. *Egg-box junction model:* the classical egg-box model illustrating the coordination of the guluronate units around the calcium ions. Oxygen atoms highlighted in orange are those involved in coordination with Ca^{2+}. Adapted from Refs[9,44]

MATERIALS AND METHODS

Materials

Partially acid hydrolyzed, high guluronate alginate originating from *Laminaria hyperborea* stipes was obtained from FMC Biopolymer, Norway. The fraction of guluronate residues (F_G) of 0.90 was confirmed by NMR (see below). Dextran T-2000 (M_w = 2 000 kDa) was purchased from Pharmacia Fine Chemical. O,O′-1,3,-propanediyl-bishydroxylamine dihydrochloride (PDHA) and 2-methyl-pyridine borane complex (PB) were purchased from Sigma-Aldrich and used as received. Deuterium oxide (D_2O) (99.90 atom% deuterium) used for neutron scattering experiments was purchased from Eurisotop (France). All other chemicals were obtained from commercial sources and of analytical grade.

Preparation of oligoguluronate and dextran blocks.

Guluronate (Na^+ form) oligomers (G oligomers) with narrow molecular weight distributions were obtained as previously described.[45] In brief, the parent (partially hydrolyzed) alginate (DP_n

37, F_G = 0.90) was fractionated according to DP by gel filtration chromatography (GFC). Fractions were characterized by SEC-MALS (chain length and dispersity) and NMR) (Table 1). High molecular weight dextran was partially hydrolyzed in 0.05 M HCl as previously described and further fractionated according to DP by GFC.[28] Narrow molecular weight dextran fractions were selected and characterized by SEC-MALS (Table 1 and Figure S1).

Preparation of PDHA-conjugates dextran

PDHA-conjugated dextran oligomers were prepared according to a previously reported method.[26,28] In brief, amination at the reducing end of dextran with excess PDHA (10 equiv.) was performed in a 500 mM sodium acetate (NaAc) buffer pH 4.0 at room temperature. After 24 h, PB was added (20 equiv.) and the reaction was continued at 40°C for 24 h. The reaction mixture was subsequently terminated by dialysis (3.5 kDa MWCO) and freeze dried. Narrow dextran-PDHA fractions were subsequently obtained by GFC. Fractions were pooled according to elution volume, dialyzed, freeze dried, and characterized by NMR and by SEC-MALS (Table 1 and Figure S1).

Preparation of G_m-b-Dex_n block copolysaccharides

The *G_m-b-Dex_n* diblocks were prepared as previously described.[28] The m and n valuers refer to DP_n values determined for each block prior to coupling. In brief, oligoguluronate blocks (21 mM) were added to 3 equiv. of PDHA-dextran dissolved in 500 mM NaAc pH 4. After 24 h, PB (3 equiv.) was added, and the reaction was left on shaking at room temperature for 120 h. The reaction mixture was dialyzed and freeze dried, before excess PDHA-dextran was removed by GFC or selective extraction with ethanol. Finally, fractions corresponding to the diblock were pooled, dialyzed and freeze dried. The purified block copolysaccharides were analyzed by NMR and by SEC-MALS (Table 1 and Figures S1-S3). A small fraction of free Dex_{51}-PDHA (< 10 wt.%) was

detected by SEC-MALS, which should not affect the block copolymer self-assembly due to its non-interacting behavior with divalent ions (Figure S1.b).

Semi-preparative gel filtration chromatography (GFC)

GFC was performed on three Superdex 30 (preparative grade) columns (HiLoad 26/ 60, 26 mm × 60 cm, GE Healthcare Life sciences) connected in series. Alternatively, for higher separation capacity, two serially connected columns (same packing material) BPG 140/950 were used. The mobile phase (0.1 M ammonium acetate (AmAc, pH 6.9) was eluted at a flow rate of 0.8 $mL.min^{-1}$ (20 $mL.min^{-1}$ for the larger columns). Samples (1.0 – 50 $mg.mL^{-1}$) were dissolved in the mobile phase and injected. The separation was monitored by an on-line RI detector (Shodex R1-101). Fractions were pooled according to elution volume. Fractions were dialyzed against 50 mM NaCl (2 shifts) and milliQ water until the conductivity was below 2 $\mu S.cm^{-1}$ and freeze-dried.

Nuclear magnetic resonance (NMR)

Polysaccharide samples were dissolved in 500 µl D_2O (99.9% D; Sigma-Aldrich) (10 – 12 mg/ml). For samples where pD was adjusted, DCl or NaOD was used. Samples were either analyzed at the temperature 25 °C, 27 °C, or 82 °C. Analyses were performed on a Bruker Ascend 600 MHz instrument equipped with Avance NEO electronics and a 5-mm Z-gradient CP- TCI cryogenic probe. All data were recorded, processed, and analysed using TopSpin software version 3.5pl7 or 3.6.1 (Bruker BioSpin).

Size exclusion chromatography with multi-angle light scattering (SEC-MALS)

Molar masses were analyzed by size exclusion chromatography with multiangle light scattering detection). The samples (1 – 3 $mg.mL^{-1}$) were dissolved in the mobile phase (0.15 M $NaNO_3$ with 10 mM EDTA) and filtered (0.45 µm) prior to injection. An Agilent Technologies 1260 IsoPump with a 1260 HiP degasser was used to maintain a flow of 0.5 $mL.min^{-1}$. Volumes of 50 – 100 µL

were injected from an Agilent Technologies Vialsampler. TSK Gel columns 4000 and 2500 PWXL were connected in series. A DAWN Heleos-II detector from Wyatt Technology was connected in series with a Shodex refractive index detector (RI-5011). Astra 7.3.2 software was used for data collection and processing. Molar masses of G_m and Dex_n precursors, Dex-PDHA and G_m-*b*-Dex_n copolysaccharides are given in Table 1. The values of refractive index increment (dn/dc in $mL.g^{-1}$) used for MALS analysis were 0.150 and 0.148 for for G_m and Dex_n, respectively. No significant variation of the dn/dc value of dextran was found for molar mass ranging 5,000 from 20,000 g/mol (data not shown). Second virial coefficients (A_2) were taken to be 5.0×10^{-3} and 2.0×10^{-4} $mL.mol.g^{-2}$ for alginate and dextran, respectively. For block copolysaccharides, dn/dc and A_2 values were averaged according to the mass composition of the copolymers. The cross-interaction term was not considered for A_2 due to negligible interaction between G_m and Dex_n blocks.

High-performance anion-exchange chromatography/pulsed amperometric detection (HPAEC-PAD)

The chain length distribution of oligoguluronates was determined by HPAEC-PAD essentially as described by Aarstad et *al.*[46] (Figure S4). In brief, samples were dissolved in water (0.1 – 1 mg/ml) injected into a Dionex BioLC system (Dionex, Sunnyvale, CA) equipped with an Dionex IonPac AS4A (4 x 250 mm) anion exchange column connected to an IonPac AG4A (4 x 50 mm) guard column. The system was eluted with a linear gradient of 8.75 mM sodium acetate in 100 mM NaOH. Data acquisition and analysis were performed using Chromeleon 6.6. software.

Table 1. Molar mass averages of G_m-*b*-Dex_n block copolysaccharides (after purification by GFC) and the corresponding starting materials (G_m and Dex_n-PDHA) and other oligoguluronates used in

the study. Molecular weights were obtained by SEC-MALS or for the lowest DPs also by HPAED-PAD. Subscripts (G_{12} etc.) refer to the DP_n values. Chromatograms are given in the Supporting Information (Figures S1-S3).

	M_n (kDa)	M_w (kDa)	DP_n (HPAEC-PAD)
G_{12}	2.0	2.0	12 (2.3 kDa)
G_{15}	3.0	3.0	15 (3.0 kDa)
G_{19}	3.8	3.8	
G_{37}	7.5	7.9	
Dex_{45}-PDHA	7.4	7.4	
Dex_{51}-PDHA	8.3	8.5	
G_{12}-*b*-Dex_{51}	12.4	12.8	
G_{19}-*b*-Dex_{45}	11.1	11.6	
G_{37}-*b*-Dex_{51}	17.0	18.7	

Dialysis cell device

A dedicated device made in PEEK was designed in collaboration with the large-scale structures group at the Laue Langevin Institute (ILL) to conduct SANS measurements during dialysis (Figure 1 and Figure S5).[43] The central part consists of a discoid scattering cell of 4.5 mL with two quartz windows, creating a measurement path that can be adjusted to either 1 or 2 mm. Two slits on the side allow ion exchange to take place through an ultrafiltration membrane of defined porosity (Millipore). Two lateral tanks of 250 mL each containing the exchange solution of divalent ions are connected to the cell. Two holes drilled on the top of the cell allow the filling and removal of the sample and also the insertion of a conductivity probe. The copolysaccharide solution in the cell and the salt solution in the reservoir are continuously homogenized under magnetic stirring during the dialysis. A temperature-controlled PMMA housing can simultaneously host three dialysis cells. In a typical dialysis experiment, a solution of block copolysaccharides at 4 $g.L^{-1}$ in 10 mM NaCl

was dialyzed at 25°C against 2 x 100 mL of 20 mM solution of divalent ions containing 10 mM NaCl. Deuterated water was systematically used for SANS dialysis experiments.

In situ time-resolved Dynamic Light Scattering (DLS)

In situ time-resolved DLS experiments were performed with a Vasco Kin™ device (Cordouan Technologies) equipped with a contactless remote head operating at a wavelength of 638 nm with a detection angle at 170° (back-scattering). The remote head was positioned at an incident angle of 30° to the dialysis cell window in order to prevent back reflection (Figure S5). The light scattering signal was acquired continuously during the whole dialysis period and then processed using NanoKin™ software (Cordouan Technologies). The time-resolved light scattering raw data were first sliced into equals periods of time, then the correlation functions were fitted using a continuous multimodal analysis algorithm named Sparse Bayesian Learning (SBL) to access the intensity-weighted particle size distribution.

In situ time-resolved Small Angle Neutron Scattering (SANS)

SANS is a perfect technique to obtain structural information of any type of particles in the range of Å up to micrometer size. The principle of SANS can be found in the following reference.[47] Briefly, a collimated neutron beam impinges a solution sample through an aperture of 13 mm diameter and the scattered intensity is recorded as a function of the scattering angle θ, such that the momentum transfer q is defined as $q = \frac{4\pi}{\lambda} sin\left(\frac{\theta}{2}\right)$ where λ is the neutron wavelength. In situ time-resolved SANS experiments were performed during dialysis on the D22 SANS spectrometer at the ILL. The wavelength was set at 6 Å and the collimation at 17.6 m, with detector distances of 17.6 m and 1.4 m for the two detectors allowing to capture a dynamic q range of 0.003 up to 0.6 $Å^{-1}$ in a single shot. The intensity presented in absolute units is obtained after correction by the

empty sample container, the blocked beam, the sample transmission, and incoming neutron flux through a direct beam measurement. Data reduction was performed using Grasp.

SANS data were fitted using the SASVIEW software with a sphere form factor:[48]

$$I(q) = \frac{scale}{V}\left[3\,V\,\Delta\rho\,\frac{\sin(qr) - qr\cos(qr)}{qr^3}\right]^2 + background$$

where the $scale$ is the volume fraction of spheres, V is the volume of the spheres, r is the radius of the spheres and the $background$ is the intensity due to incoherent scattering. $\Delta\rho$ is the scattering length density (SLD) difference between the scatterer and the solvent (D_2O). The $background$ value was imposed for each SANS curve from the readout value of the intensity at high q. The scale linked to the assumed constant volume fraction was set. The two fitted parameters were then the SLD and the radius of the spheres. A Gaussian polydispersity function was set manually (associated with the standard deviation σ). The acquisition of the spectra during the dialysis was performed in 5-minute slices every 15 minutes in order to allow the simultaneous acquisition of three dialysis cells placed on a dedicated sample holder including dedicated stirring units.

Batch Static and Dynamic Light Scattering (SLS and DLS)

Multiangle static and dynamic light scattering (SLS, DLS) experiments in batch mode were performed using an ALV/CGS3 compact goniometer equipped with an ALV/LSE-5004 light scattering electronics and an ALV-7004 multi tau digital correlator with pseudo-cross correlation detection. The light source was a 22 mW He-Ne laser operating at λ_0 = 632.8 nm. Measurements were carried out at 25°C. For static light scattering analysis of micellar nanogels, the scattered intensities at multiple angles and various concentrations were analyzed according to the Rayleigh-Gans-Debye (RGD) equation by plotting the logarithm of the reciprocal of the scattering intensity against $q^2 + kc$ (Guinier modification of the Zimm plot)[49] which provided best data linearization:

$$\ln\left(\frac{Kc}{\Delta R}\right) = \ln\left(\frac{1}{M_w\left(e^{-\frac{1}{3}R_g^2 q^2}\right)} + 2A_2 c\right)$$

with ΔR the excess Rayleigh ratio, c the mass concentration, M_w the weight-average molecular weight, R_g the z-average radius of gyration, A_2 the z-average second virial coefficient, q the magnitude of the scattering vector and K the optical constant (contrast factor) where $K = 4\pi^2 n_0^2 (dn/dc)^2 / \lambda_0^4 N_A$ with n_0 the refractive index of the solvent, (dn/dc) the refractive index increment, N_A the Avogadro number and λ_0 the vacuum wavelength of the primary beam. The excess Rayleigh ratio was obtained at various concentrations and detection angles according to:

$$\Delta R = \frac{I - I_0}{I_T}\left(\frac{n_0}{n_T}\right)^2 R_T$$

with I, I_0, I_T the scattered intensities of the particle dispersion, solvent and toluene measured at varying scattering angle θ and R_T the Rayleigh ratio of toluene (1.355 x 10^{-5} cm^{-1}).[50] The RGD equation applies when $qR_G \ll 1$ (Guinier regime), that is, for particles of smaller size than the observation scale (q^{-1}). The refractive index increment of polymer particles dn/dc was determined with a differential refractive index detector (Optilab rEX, Wyatt Technology) working at λ_0 = 658 nm. The suspension of block copolysaccharide nanogels collected after dialysis was diluted at different concentrations with 20 mM $CaCl_2$ + 10 mM NaCl and dialyzed again against same solution to equilibrate the chemical potential prior to dn/dc determination.

For DLS measurements, the normalized time autocorrelation functions of the scattered light intensity obtained at various angles (40° to 150°) were fitted with the constrained regularization method (CONTIN) which provides the distribution of relaxation times (τ). A single relaxation mode was found at each angle. Then, the z-average of the apparent mutual diffusion coefficient ($D_{app,z}$) of polymer particles was determined by plotting Γ, the decay time (relaxation rate, τ^{-1}) as

function of the squared scattering vector (q^2). A linear plot was found from which $D_{app,z}$ can be derived, $D_{app,z} = \Gamma/q^2$. The apparent z-average of the hydrodynamic radius ($R_{H,z}$) was calculated according to the Stokes-Einstein equation:

$$R_H = \frac{k_B T}{6\pi\eta D_{app}}$$

where k_B is the Boltzmann constant, T the temperature and η the viscosity of the solvent.

Atomic force microscopy (AFM)

AFM measurements were performed at room temperature in the dry state using a Multimode 8™ microscope (Bruker Instruments Inc.). Topographic images of individual particles were obtained in tapping mode using a rectangular silicon cantilever (AC 160-TS, Atomic Force, Germany) with a spring constant of 26 $N.m^{-1}$, a resonance frequency in the range of 270-320 kHz and a radius of curvature of less than 10 nm. A drop (4 µL) of the suspension of block copolysaccharide particles, initially at 3.5 $g.L^{-1}$ and diluted with water to 0.01 $g.L^{-1}$, was deposited with a micropipette onto freshly cleaved mica and allowed to dry under nitrogen flow. Height measurements were performed using the section Particle Analysis tool provided with the AFM software (Nanoscope Analysis V1.20 from Bruker).

RESULTS

1. Block copolysaccharide self-assembly through dialysis against divalent ion solutions.

Oligoguluronate-*b*-dextran (G_m-*b*-Dex_n) block copolysaccharides, initially in the water-soluble sodium form, were self-assembled with various divalent ions (Ca^{2+}, Ba^{2+}, Sr^{2+}). Due to strong interaction between divalent cations and G blocks, the self-assembly was performed under defined kinetic conditions using a dedicated dialysis setup allowing slow and controlled ion diffusion at constant polymer concentration (Figure 1).[43] Under such conditions, the self-assembly can be

performed near thermodynamic equilibrium, thereby preventing the formation of multiple metastable states, as often observed with amphiphilic block copolymers.[38,41,51] In situ time-resolved dynamic light scattering (Tr-DLS) and small-angle neutron scattering (Tr-SANS) were conducted to monitor structural changes in copolysaccharide solution during dialysis.

Determining the ion concentration in the cell during dialysis is not straightforward, as guluronate units interact with divalent ions as they diffuse into the cell. However, the ion diffusion kinetics could be estimated from conductivity measurements in the absence of copolymer (Figure S6). The concentration of divalent ions in the reservoirs and the molecular weight cut-off (MWCO) of the cellulose membrane were then optimized to achieve block copolymer self-assembly in a few hours. Faster or slower ion diffusion can be performed by using larger or smaller MWCOs (Figure S6). Two block copolysaccharide compositions, G_{12}-*b*-Dex_{51} and G_{37}-*b*-Dex_{51} were selected to specifically study the influence of the complexing block (G) length on the characteristics of the self-assembled structures formed.

Dialysis monitoring by Tr-DLS. Starting with the G_{37}-*b*-Dex_{51} dissolved at a concentration of 4 $g.L^{-1}$ (9.4 mM in G units) in 10 mM NaCl, the copolysaccharide response to calcium ions was first studied by in-situ Tr-DLS. Initially, the scattering intensity and the intercept on the correlograms were low due to the relatively low polymer concentration and molar mass (Figure S7A). Under such conditions, the size distribution was noisy with a diversity of relaxation modes, probably due to the polyelectrolyte behavior of the G block (Figure 2A).[52] Nevertheless, an abrupt change in scattering properties was observed around 180 minutes, as shown from the net increase of the intercept on correlation curves (Figure S7A). The delay time illustrates the slow diffusion of divalent ions through the semi-permeable membrane before the critical ion concentration to trigger copolysaccharide self-assembly was reached. From there, one could detect a main

population of particles with a radius close to 30 nm accompanied by a small fraction of aggregates larger than 50 nm (Figure 2A). The size of these two populations progressively increased with time as calcium ions diffused in the cell, thus emphasizing the limited stability of the particles formed. The formation of large aggregate structures was demonstrated by SANS under similar experimental conditions (Figure S8A) and by analyzing the solution collected at the end of the dialysis with a different DLS instrument (Figure S8B). Therefore, the block size ratio of G_{37}-*b*-Dex_{51} was not appropriate to form stable micellar structures.

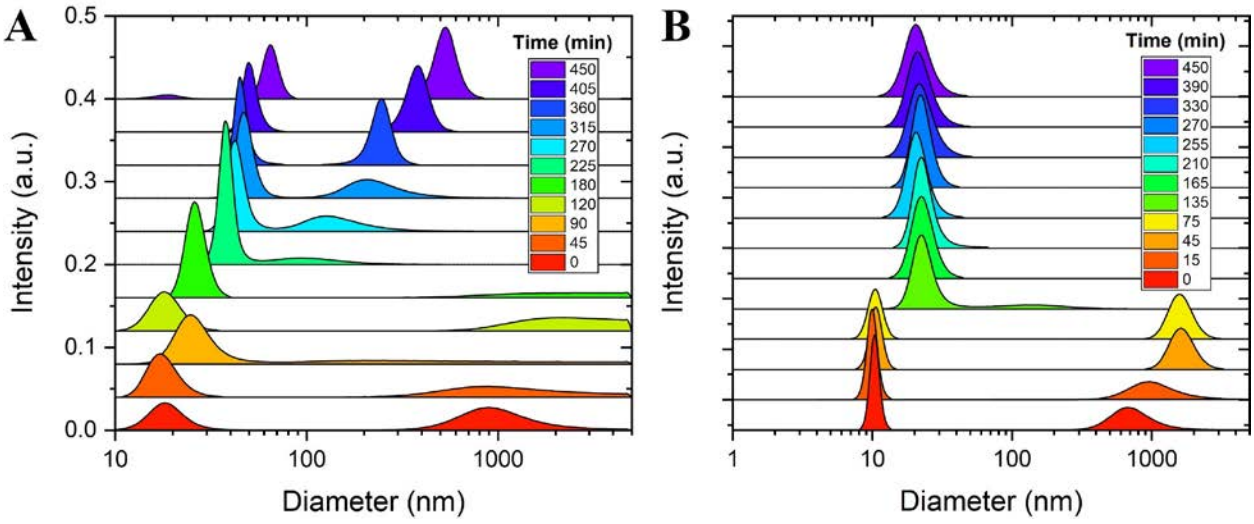

Figure 2. Time-resolved DLS monitoring of the dialysis of G_m-*b*-Dex_n against calcium ion solution for two block copolysaccharide compositions: A) G_{37}-*b*-Dex_{51}. B) G_{12}-*b*-Dex_{51}. Intensity-weighted size distributions are plotted at different dialysis times. Copolymer were dissolved at 4 $g.L^{-1}$ in 10 mM NaCl. The dialysis was performed against 2 x 100 mL of 20 mM $CaCl_2$ in 10 mM NaCl using a dialysis membrane with a MWCO of 10 kDa.

With the shorter G_{12}-*b*-Dex_{51} copolymer dissolved at a concentration of 4 gL^{-1} (4.5 mM in G units) in 10 mM NaCl, the trend observed in DLS was somewhat different (Figure 2B). First, two

distinct relaxation modes corresponding to free copolymer chains and some aggregates could be clearly observed at early stages of the dialysis. After 120 minutes, a subtle change was observed in the size distribution with the population of free copolymer chains disappearing and a new population with a slightly larger radius appearing (around 20 nm in diameter). This population corresponding to the expected micellar nanogels persisted until the end of the dialysis. In the meantime, the aggregate fraction decreased considerably and ultimately reached near-negligible levels by the end of the dialysis.

Dialysis monitoring by Tr-SANS. In order to gain further insight into nanogel formation, *in situ* Tr-SANS experiment was conducted under similar dialysis conditions on G_{12}-*b*-Dex_{51} with calcium, strontium, and barium ions. The scattering intensity at the beginning of the dialysis was low and spectra difficult to fit. However, consistent with the previous DLS analysis, the intensity markedly increased after a delay of 80 to 120 minutes required to reach the Critical Ion Concentration (CIC) (Figures 3A-C). A simple sphere model was used to fit the SANS spectra, yielding better results compared to a core-shell model previously used for DHBC micelles.[53] This indicates that the scattering intensity mainly originated from the G blocks forming the particle core, the contribution of the hydrated dextran shell being negligible. The size (radius, r) and the scattering length density (SLD) of particles were fitted and plotted in Figures 3D-F (see also data in Figures S9-S11 and Tables S1-S3). The particles rapidly achieved their equilibrium size ($r < 8$ nm), which is consistent with a closed-association model in which micellar structures of finite size are formed once self-assembly conditions are met. The decrease in the scattering length density (SLD) of particles over time, alongside the increase in scattering intensity was more intriguing. Given that the volume fraction of the spheres was held constant in the fitting procedure, the increase in scattering intensity must be attributed to an increase in the contrast term, $(\Delta\rho)^2 =$

$(\rho_{part.} - \rho_{D2O})^2$ where ρ represents the corresponding SLD values. Since the SLD of sodium and calcium ions are similar, the change in contrast could not be attributed to a simple ion exchange (Table S4). Instead, it can be assumed that water molecules initially bound to the G units were released upon complexation with divalent ions. Consequently, the SLD of particles was expressed as: $\rho_{part.} = \psi * \rho_{D2O} + (1 - \psi) * \rho_G$ with ψ representing the volume fraction of water molecules bound to G units, and ρ_{D2O} and ρ_G the SLD of D_2O and G blocks, respectively. Under these conditions, the SLD of the particles must decrease over time while the contrast and scattering intensity simultaneously increased. Interestingly, the decrease in SLD continued to some extent beyond the achievement of equilibrium particle size, particularly with calcium, indicating the completion of the complexation process (Figure 3D). The particle compactness estimated from radius measurements at equilibrium as well as the dehydration rate (k) increased in the order of $Ca^{2+} < Sr^{2+} < Ba^{2+}$, in agreement with the respective affinity of divalent ions with G blocks.[5]

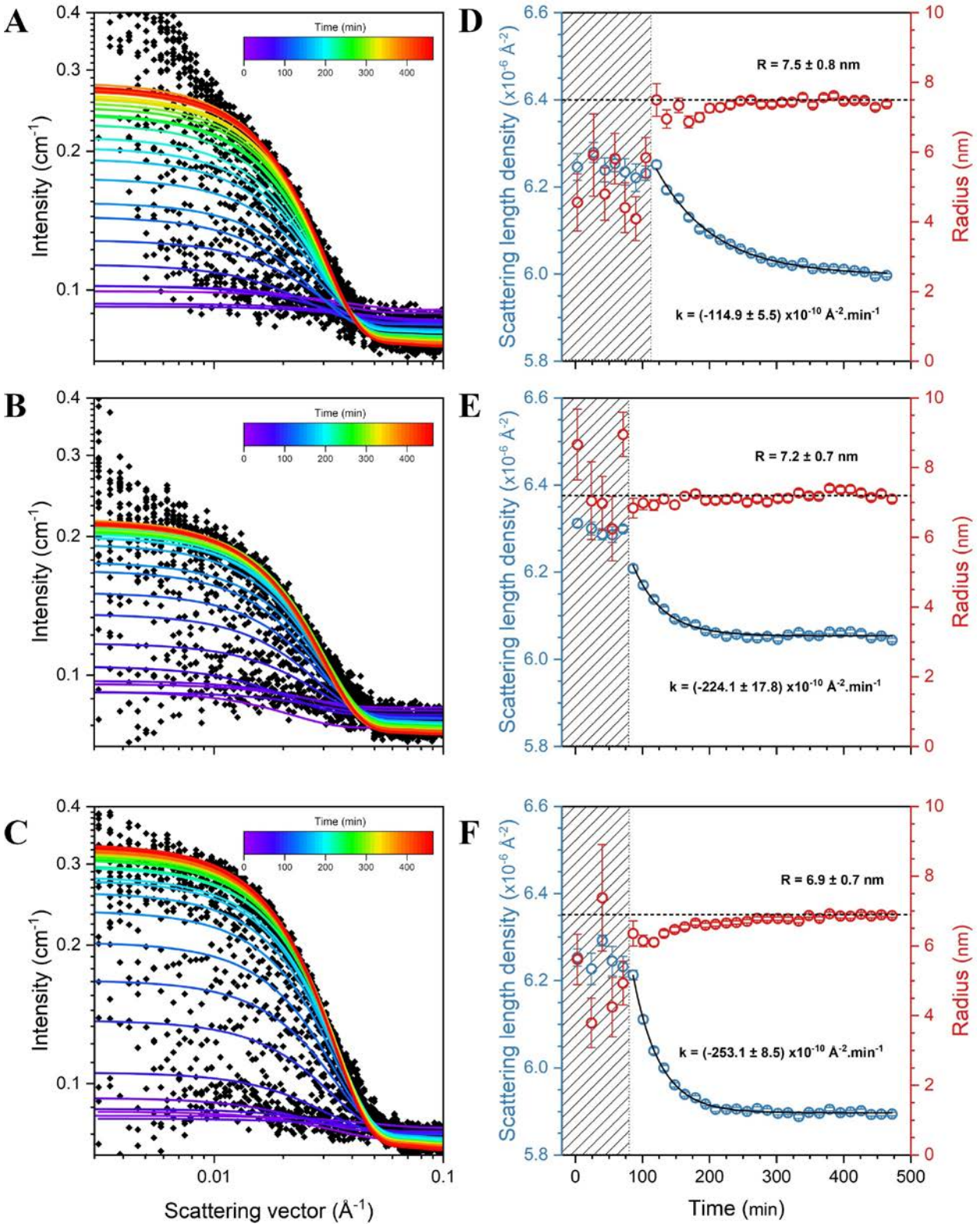
A
B
C
D
E
F
Time (min)
0
100
200
300
400
Intensity (cm^{-1})
Scattering vector (Å^{-1})
0.01
0.1
Scattering length density (x10^{-6} Å^{-2})
Radius (nm)
Time (min)
R = 7.5 ± 0.8 nm
k = (-114.9 ± 5.5) x10^{-10} Å^{-2}.min^{-1}
R = 7.2 ± 0.7 nm
k = (-224.1 ± 17.8) x10^{-10} Å^{-2}.min^{-1}
R = 6.9 ± 0.7 nm
k = (-253.1 ± 8.5) x10^{-10} Å^{-2}.min^{-1}

Figure 3. Time-resolved SANS monitoring of the dialysis self-assembly of G_{12}-*b*-Dex_{51} in presence of calcium (A, D), strontium (B, E) and barium (C, F) ions. A-C) Coherent neutron scattering intensity versus scattering wave-vector at different dialysis times. See also Figures S9-S11 for individual spectra. D-F) Radius (red) and scattering length density (blue) of particles. Dotted lines show the final radius of the particles. The rate constant k associated to the variation of the SLD of particles (black line) was determined using a single exponential expression: $SLD = SLD_0 + Ae^{-kt}$. Experimental conditions similar to those reported in Figure 2 were used. The upturn of the scattered intensity observed with calcium at the low *q*-end (Figure 3A), which was not detected with barium and strontium may indicate that the copolymer was not fully solubilized for this dialysis experiment (no upturn was observed in the calcium dialysis preceding EDTA exchange, as shown in Figures 7B and S15). Nonetheless, the scattering due to particle formation was mainly detected in the intermediate q range and could be adequately fitted.

After dialysis against calcium ion solution, G_{12}-*b*-Dex_{51} micelles were further characterized by AFM, static and dynamic multi-angle light scattering (Figure 4 and Table 2). AFM revealed the presence of well-defined spherical particles with an average radius of 10 nm in the dry state, a value close to that found by SANS (Figure 4A). Static light scattering (SLS) (Figure 4B) afforded a weight-average molar mass (M_W) of 270 000 g/mol corresponding to an aggregation number ($N_{agg,w}$) of 21, neglecting the contribution of calcium ions (< 2 wt.%). The second virial coefficient of micelles was found to be positive but lower than for alginates in solution (*ca* 5×10^{-3} mL.mol.g^{-2} at I = 0.17 M),[54] indicating that Donnan effects originating from the polyelectrolyte behavior of the oligoguluronate chains were largely cancelled due to binding of calcium ions. The radius of gyration (R_G) of micelles could not be determined by SLS due to the low angular dependency of the scattering intensity in relation with the small particle size in comparison to the wavelength of light ($r < \lambda_0/20$). However, R_G could be determined by fitting the SANS scattering profiles at low q with the Guinier approximation $I(q) = I(0)\exp\left(-\frac{q^2R_G^2}{3}\right)$. A value of R_G = 5.4 nm was obtained from the data in Figure 7B, where no upturn of the scattered intensity was observed at low q. Multiangle DLS analysis demonstrated the purely diffusive behavior of micelles as well as the absence of significant size dispersity or other relaxation mechanisms, as judged by the linearity of the $\Gamma(q^2)$ plot (Figure 4C). The hydrodynamic radius (R_H) derived from the Stokes-Einstein equation was found to be 9.5 nm (Table 2). The R_G/R_H ratio which represents the Burchard shape factor (ρ)[55] was then equal to 0.57. This suggests that micellar nanogels obtained from G_{12}-*b*-Dex_{51} have a star-like morphology, consistent with the significant larger size of the dextran blocks. Sanson *et al.* found a rather similar ρ value of 0.50 for PAA_{3000}-*b*-PAM_{15000} double hydrophilic copolymer complexed with aluminum ions.[53] Given the low aggregation number and the small size of the G blocks, the radius of 7.5 nm determined by SANS for calcium dialysis may be

overestimated, suggesting that the contribution of dextran segments at the core surface may have been included in the spherical model. Applying a core-shell or fuzzy sphere model would be more appropriate for determining the characteristic micelle sizes. However, this approach would require enhanced data statistics, necessitating longer acquisition times. Consequently, this would reduce the sampling frequency, particularly since three dialysis experiments were analyzed simultaneously.

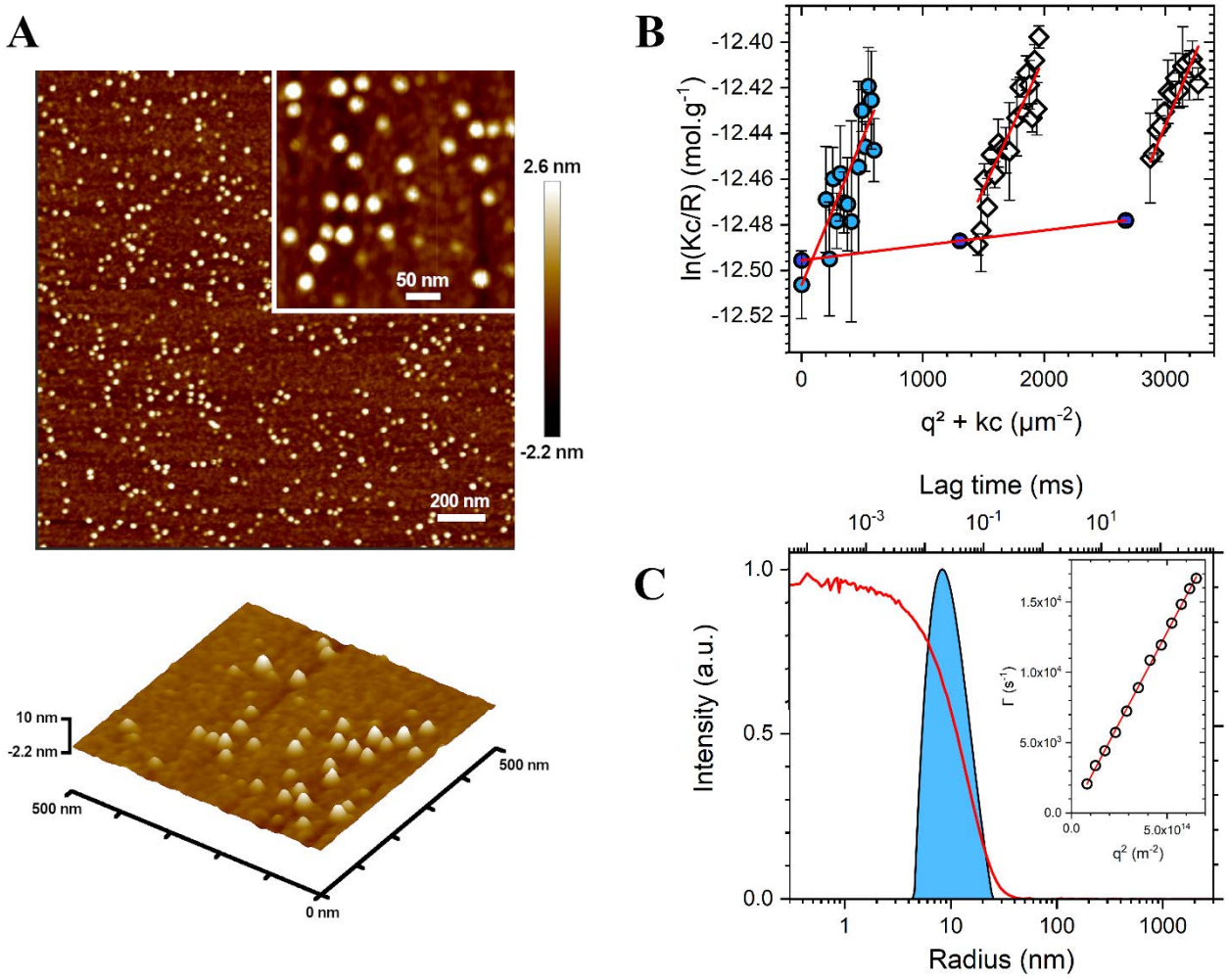

Figure 4. Characterization of micellar nanogels obtained from dialysis of G_{12}-*b*-Dex_{51} against calcium ions. A) 2D image by AFM scanning of mica surface (2 µm x 2 µm) (top). 3D image corresponding to the sample section shown (bottom). B) Guinier-Zimm plot obtained by SLS. k is a geometric constant. C) DLS analysis at 90°; the inset shows the $\Gamma(q^2)$ variation.

Table 2. Main characteristics of block copolysaccharide micelles obtained from dialysis of G_{12}-*b*-Dex_{51} against calcium ions.

Technique	Parameter	Value
SANS	r	7.5 ± 1.1 nm
DLS	R_H[a]	9.5 ± 1.2 nm
	PDI[b]	0.12
SLS	dn/dc	0.1444 ± 0.0413 $mL.g^{-1}$
	M_w [c]	$2.7 \times 10^5 \pm 1.4 \times 10^4$ $g.mol^{-1}$
	$A_{2,z}$ [d]	$1.4 \times 10^{-5} \pm 7.0 \times 10^{-7}$ $mol.mL.g^{-2}$
	$N_{agg,w}$ [e]	21 ± 1.0

[a] Hydrodynamic radius (z-average) calculated from multiangle DLS analysis
[b] Polydispersity index obtained from the cumulant analysis of the correlation function at 90°
[c,d] Molar mass (weight average) and 2nd virial second coefficient (z-average) obtained from the Guinier-Zimm plot representation.
[e] Aggregation number (weight average)

Comparison with the batch addition of calcium ions. In order to precisely control the divalent ion concentration introduced, the self-assembly of G_{12}-*b*-Dex_{51} was also performed by gradual additions of known quantities of calcium to the copolymer solution under conditions otherwise identical to those for dialysis. Additions at 5-minute or 5-hour intervals, referred to as fast or slow additions in the following, were performed to investigate the equilibrium properties of the system. The formation of micellar structures was monitored through SLS and DLS and correlated to the molar mixing ratio R = $[Ca^{2+}]/[G]$ (Figure 5 and Figure S12). A control experiment was also

performed with a guluronate block of DP 15 (G_{15}). Two R values are of specific interest, namely R = 0. 25 for dimers and R = 0.50 for infinite multimers (Figure 1).[10] For G_{15} with fast additions of calcium, a sharp increase in scattering intensity was observed between R = 0.35 and R = 0.70, concomitant with the precipitation of oligomer (Figure 5A, Figure S13). Under similar conditions, the intensity increase for G_{12}-*b*-Dex_{51} was shifted to higher R ratios, indicating that the introduction of dextran blocks has imposed constraints, probably of entropic origin, on the complexation of G blocks by calcium ions. With slow calcium additions conditions that mimic those of dialysis, the block copolymer self-assembled at even higher R ratios. Aggregation number values between 16 and 19 were found for R > 5. The N_{agg} value of 2 at R=0.80 could indicate the formation of dimers or a mixture of n-mers and free copolymers (Figure 5B). The successive size distributions obtained by DLS at various R values for slow calcium additions were consistent with those obtained by dialysis (Figure 5C) as well as the R_H and PDI values obtained (Figure 5D). This result suggests that the self-assembly occurs near equilibrium conditions, regardless of the mixing process. Therefore, the characteristics of the micellar nanogels are primarily determined by the thermodynamics of assembly in relation to the block copolymer composition.

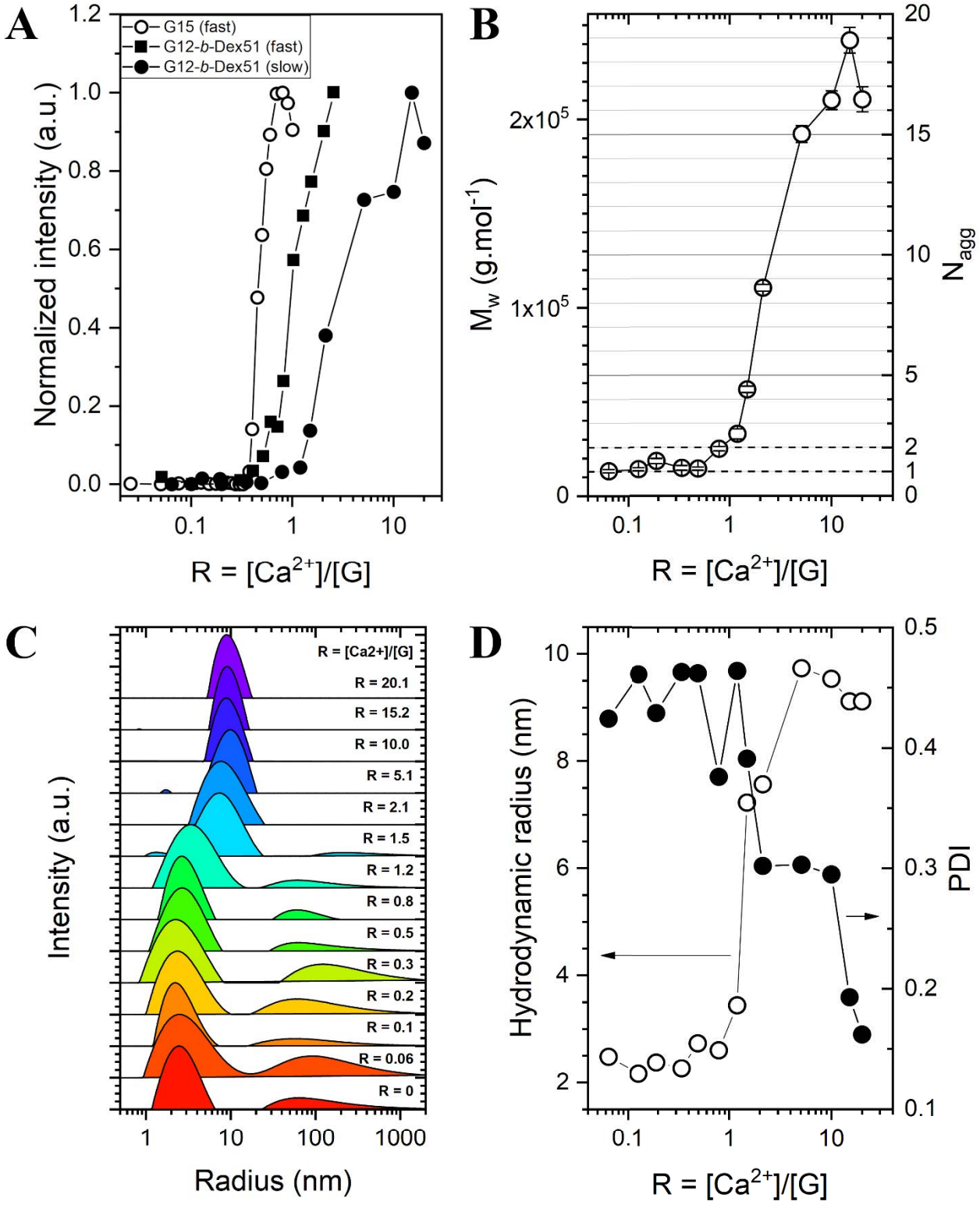
A
G15 (fast)
G12-b-Dex51 (fast)
G12-b-Dex51 (slow)
Normalized intensity (a.u.)
R = [Ca2+]/[G]
B
Mw (g.mol-1)
Nagg
R = [Ca2+]/[G]
C
R = [Ca2+]/[G]
R = 20.1
R = 15.2
R = 10.0
R = 5.1
R = 2.1
R = 1.5
R = 1.2
R = 0.8
R = 0.5
R = 0.3
R = 0.2
R = 0.1
R = 0.06
R = 0
Intensity (a.u.)
Radius (nm)
D
Hydrodynamic radius (nm)
PDI
R = [Ca2+]/[G]

Figure 5. SLS and DLS analysis of G_{15} and G_{12}-*b*-Dex_{51} solutions at 4 $g.L^{-1}$ in 10 mM NaCl as function of R = $[Ca^{2+}]$ / [G] following successive additions of 20 mM calcium chloride solution containing 10 mM NaCl A) Normalized scattered intensity of G_{15} and G_{12}-*b*-Dex_{51} against R, with comparison of slow and fast calcium additions (see text). B) Variation of the weight-average molar mass (M_w) and aggregation number (N_{agg}) of G_{12}-*b*-Dex_{51} for slow calcium additions (see raw data in Figure S12). C) Intensity-weighted size distributions of G_{12}-*b*-Dex_{51} obtained by DLS in similar conditions. D) Intensity-weighted mean hydrodynamic radii (Z-average) and polydispersity indexes (PDI) of G_{12}-*b*-Dex_{51} against R (slow additions).

2. Stability of block copolysaccharide micelles

Ca^{2+}-micelles. The application of block copolysaccharide micelles for biomedical purposes, such as in vivo imaging, requires structural stability throughout production, purification, and application under physiological conditions. The stability of preformed G_{12}-*b*-Dex_{51} micelles by dialysis against calcium was investigated by DLS in various pH and saline conditions. They were found to be perfectly stable upon storage for up to one month in a 10 mM sodium chloride + 20 mM calcium chloride solution (Figure 6A). After freeze drying, micelles could also be easily redispersed in water without cryoprotective agents, with dextran presumably playing naturally this role (Figure 6A). When the medium was acidified to pH 1, the size of the micelles increased significantly, but the structures remained well-defined with a low PDI value (< 0.1) (Figure 6B). Free G-blocks normally precipitate at this pH but with a type of chain-chain associations not requiring Ca^{2+}.[56] The copolymer can thus remain micellized under acidic conditions, with the protonated G blocks forming the core through hydrogen bonding. However, there is a difference between the two assembly modes. At neutral pH in the presence of calcium, the core of the micelles is organized and compact due to specific chain−chain association and formation of junction zones.

In contrast, the precipitation of acidified G blocks is not controlled, with only the formation of a steric barrier of dextran blocks limiting the extent of copolymer aggregation.[57]

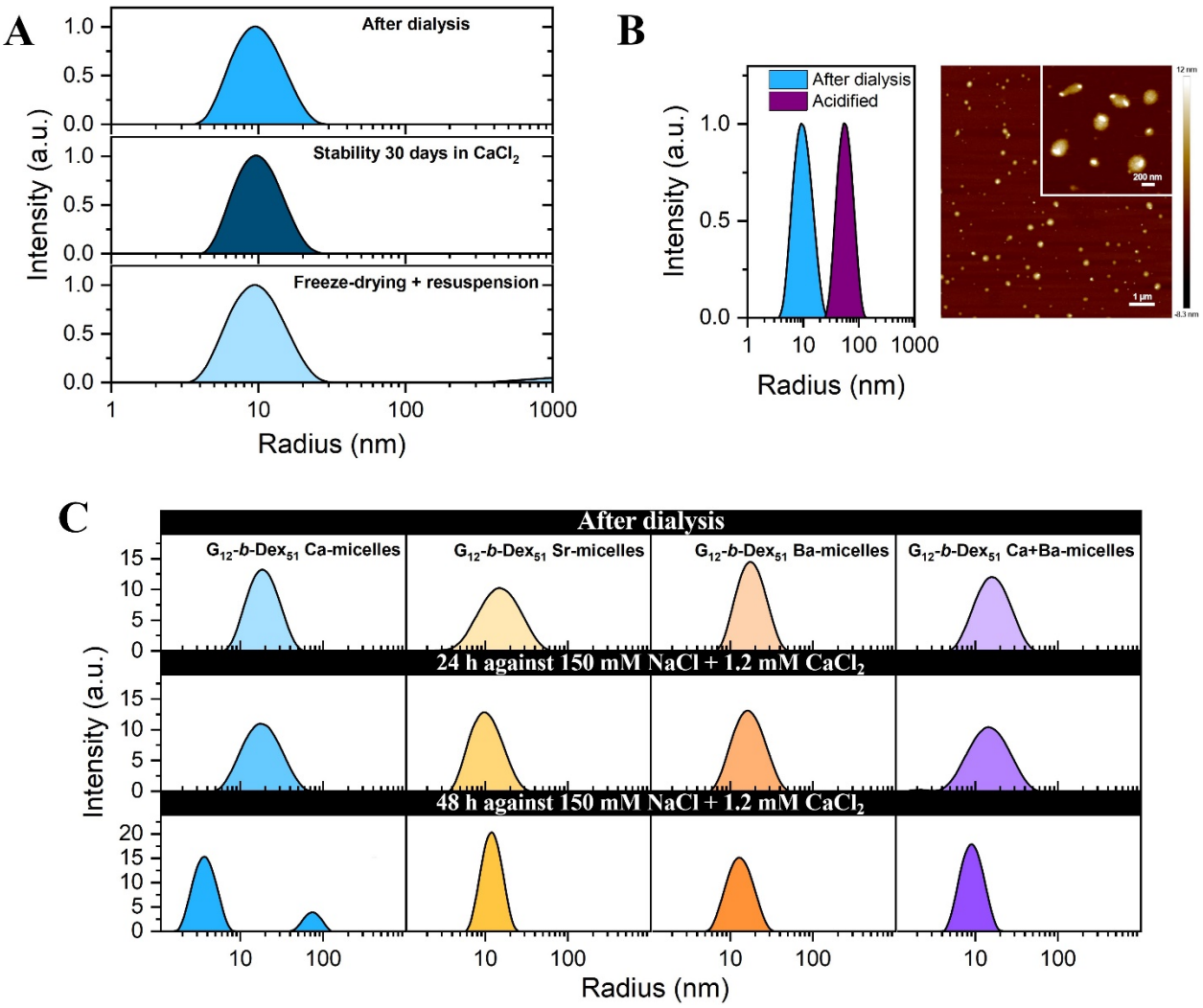

Figure 6. Stability of G_m-*b*-Dex_n micelles in various salt and pH conditions evaluated from DLS analysis. Autocorrelation functions and intensity-weighted size distributions are systematically plotted. A) G_{12}-*b*-Dex_{51} upon dialysis against 20 mM $CaCl_2$ + 10 mM NaCl: initial state, 30 days storage in same salt conditions, after freeze drying and resuspension in water (from top to bottom). B) Acidification of G_{12}-*b*-Dex_{51}/Ca^{2+} micelles at pH 1: DLS analysis (left) and AFM imaging (right). C) G_{12}-*b*-Dex_{51} micelles upon dialysis against 10 mM NaCl containing 20 mM $CaCl_2$, 20

mM $SrCl_2$, 20 mM $BaCl_2$ or 19 mM $CaCl_2$ +1 mM $BaCl_2$ (top). Same samples after 24 h (middle) and 48 h (bottom) dialysis against physiological saline (1.2 mM $CaCl_2$ in 150 mM NaCl).

When dialyzed against 150 mM NaCl the G_{12}-*b*-Dex_{51}/Ca^{2+} micelles disintegrated rapidly (Figure S14A). Including 1.2 mM $CaCl_2$ (physiological conditions) delayed the disintegration somewhat but not sufficiently for most practical applications (Figure S14A). This is in line with the observation that calcium alginate gels swell and eventually dissolve under physiological condition due to continuous Ca-Na exchange.[58] To obtain more robust micelles we reasoned that longer G-blocks were necessary and therefore included G_{19}-*b*-Dex_{45} in the study. The micelles obtained with this copolymer composition remained stable for over 6 days when dialyzed against 150 mM NaCl containing 1.2 mM $CaCl_2$ (Figure S14B). However, some large aggregates were noticed, albeit in smaller amounts as compared to G_{37}-*b*-Dex_{51} (Figure 2A).

Sr^{2+}- and Ba^{2+}-micelles. Another strategy to obtain stronger chain-chain interactions with G_{12}-*b*-Dex_{51} consists in replacing the calcium by strontium and barium salts. Both Sr^{2+} and Ba^{2+} bind stronger to alginates than do Ca^{2+}.[5] G_{12}-*b*-Dex_{51} was therefore dialyzed (3.5 kDa MWCO) against 10 mM NaCl containing 20 mM of $CaCl_2$, $SrCl_2$, $BaCl_2$ or 19 mM $CaCl_2$ +1 mM $BaCl_2$. All systems formed well-defined micelles of small size according to DLS analysis (Figure 6C). The micelles were further dialyzed against 1.2 mM $CaCl_2$, 150 mM NaCl. When monitored after 24 h only minor changes in micelle dimensions were observed, but after 48 h the micelles prepared only with calcium had disintegrated as the size distribution approached that of free copolymers in solution (Figure S14). In contrast, micelles formed with Sr^{2+} or Ba^{2+}, or with Ca^{2+} in the presence of only 1 mM Ba^{2+}, remained stable. Hence, Sr^{2+} and Ba^{2+}, significantly enhance the stabilization of the micelles due to their stronger binding with alginates.

Ion exchange and competitive chelation properties. Tr-SANS was performed to study ion exchange and chelation by multidentate ligands when preformed Ca-micelles are dialyzed against barium ions and sodium EDTA, respectively. In the first case, at the end of the dialysis of the copolymer against $CaCl_2$ (Figure 3A), the content of the two reservoirs was replaced by a 20 mM $BaCl_2$ in 10 mM NaCl solution. The scattering intensity immediately increased without delay time indicating that ion exchange is occurring in the core of micelles rather than a disassembly/assembly process (Figure 7A and Figure S15). The increase in intensity can be attributed to the formation of denser structures by compaction of the micelle core with barium ions due to their greater affinity than calcium for G blocks, as seen previously. Consequently, a decrease in particle radius was observed (Figure 7C and Table S5). No change in particle shape and size could be observed compared to previous dialysis experiments with $BaCl_2$ (Figure 3). However, the rate constant (k) associated to the change in SLD was almost 3 times lower than that obtained for the direct dialysis against barium (Figure 7D) illustrating the competitive interaction between barium and calcium ions for G blocks. Eventually, the scattering intensity reached a plateau when the ion exchange was almost completed. It corresponds to a particle radius of (7.2 ± 0.1) nm, which is slightly larger than the radius obtained through direct dialysis against $BaCl_2$ (6.9 nm) (Figure 3F). In the second case, the content of the reservoirs was replaced by an 80 mM EDTA solution. The scattering intensity immediately started to decrease (Figure 7B and Figure S16) but was accompanied by an increase in particle size (Figure 7C and Table S6). This is consistent with a disassembly mechanism where the micelles first swell as the EDTA chelates the calcium ions (exchange with Na^+), forming loose structures and progressively releasing the polymer molecules into solution. This shows that the hexadentate EDTA is a stronger ligand of calcium ions than the G_{12} block under the conditions used, in excellent agreement with the EDTA-sensitivity observed in Ca-alginate gels.[59]

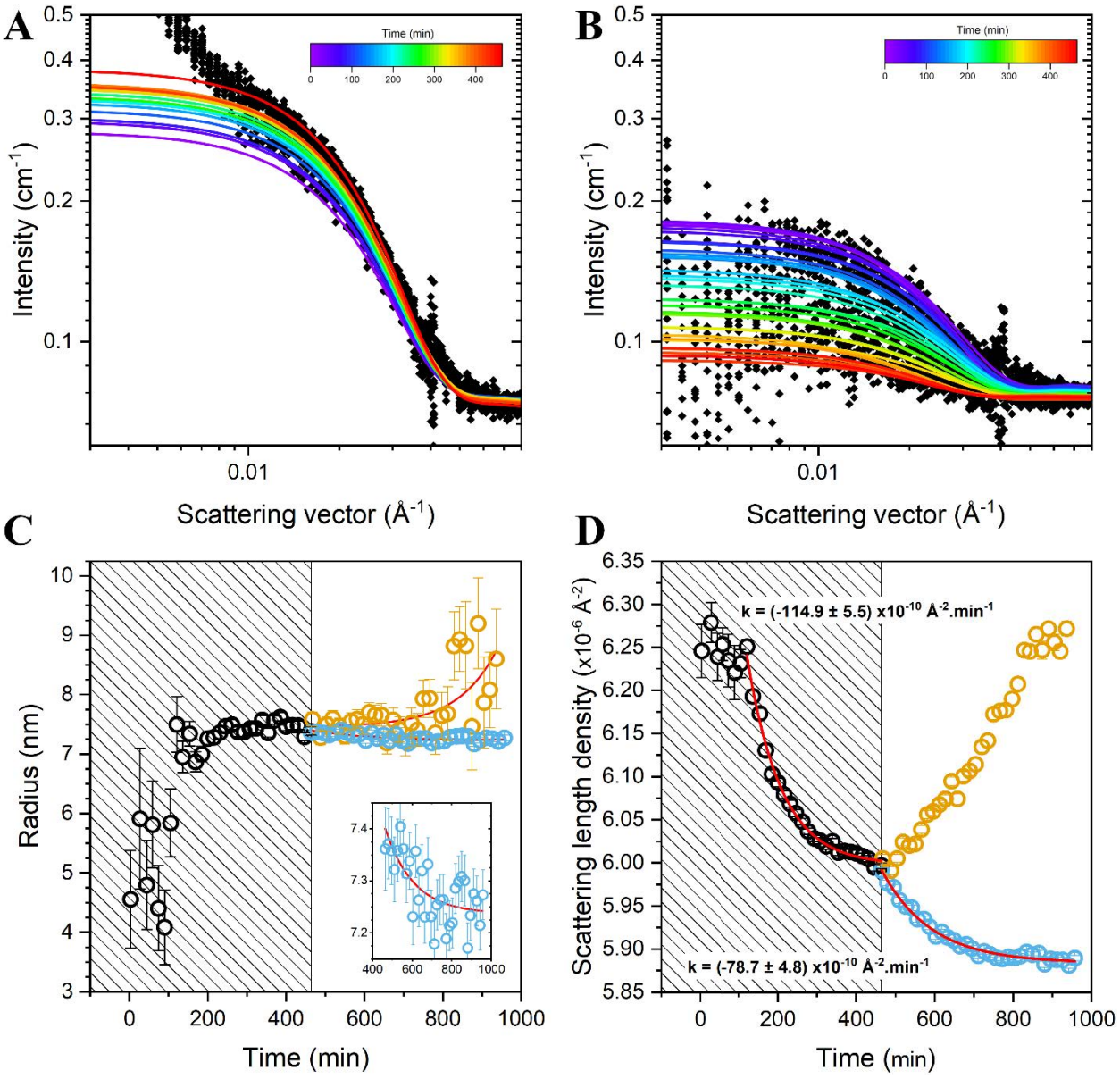

Figure 7. Ion exchange of preformed G_{12}-*b*-Dex_{51} / Ca^{2+} micelles in 20 mM $CaCl_2$ + 10 mM NaCl with 20 mM $BaCl_2$ + 10 mM NaCl (A) and 80 mM EDTA (B), as monitored by time-resolved SANS. See also Figures S15 and S16 for individual spectra The particle radius (C) and SLD (D) are plotted as function of the dialysis time for the formation of G_{12}-*b*-Dex_{51} / Ca^{2+} micelles (shaded area) followed by the exchange either with Ba^{2+} (blue) or EDTA (orange). The inset is a magnification of the size decrease of micelles upon exchange with Ba^{2+}.

DISCUSSION

The development of nanoscale alginate-based materials usually requires approaches in dispersed media or the use of microfluidic techniques to control the gelation mechanisms of alginate chains under different conditions, usually in the presence of divalent ions such as calcium. The spontaneous formation of alginate-based nanostructures, on the other hand, requires a thermodynamic approach, such as self-assembly based on the principle of molecular attraction-repulsion. In this work we demonstrate that well-defined, spherical, and stable alginate nanoparticles can be obtained from G_m-*b*-Dex_n block copolysaccharides when dialyzed against divalent alkaline earth ions such as Ca^{2+}, Sr^{2+} and Ba^{2+}. Unlike monovalent cations or divalent Mg^{2+} ions, these cations are known to bind strongly to G-blocks and further induce G-block dimerization, which subsequently leads to gelation of alginates, but precipitation of purified G-blocks.[5] Hence, the ability to self-assemble into defined nanoparticles is a new property introduced into oligoguluronates by terminal attachment of a second, non-responsive, dextran block. It is noteworthy that G-blocks interact more strongly with Ca^{2+}, Sr^{2+} and Ba^{2+} than many other carboxylated polysaccharides (hyaluronan, mannuronan ...). This is understood as two separate effects: a) charge density effects (one charge per 0.435 nm linear charge density in G block,[60] b) additional binding site effects due to the geometry of G-blocks (chelation effect) which only happens when chains dimerize with divalent ions (egg-box model). The higher affinity of calcium ions for G blocks compared to other polyacids such as PAA is clearly demonstrated, for example, by calorimetry, with an exothermic response in the former case[10] and an endothermic response in the latter case.[61,62] While alginates are stiff macromolecules due to restricted rotation around their glycosidic linkages, dextran, used here as a neutral and stabilizing block is a polymer with high chain flexibility due to α-(1→6) glycosidic linkages which contain three bonds between each pair

of glucose residues and therefore one extra single rotatory bond per monomer unit compared to α-(1→4) or β-(1→4) linkages found in most polysaccharides. The extendable coil structure of dextran should increase the aggregation number of micelles and therefore the core size by accommodating more copolymer chains. However, the flexible corona is less stable than a rigid one, making the micelle more prone to disassembly under changing conditions.

The very small size of the particles (radius < 8 nm) with a narrow size distribution, coupled with the characteristic response to G-block sensitive cations suggests a dynamic structure forming micellar aggregates. The assembly mechanism follows a closed association model, where only monomers and monodisperse micelles with a specific aggregation number are present in the solution.[63] The core consists of divalent cations chelated by oligoguluronate segments, while a corona of neutral dextran segments provides steric stabilization (Figure 3). The small size is consistent with the low aggregation number (N_{agg} ~ 20) obtained by static light scattering (Table 2). Given that the micelle core originates from a gelation process, the term "micellar nanogel" appears appropriate for characterizing the structures obtained. A star-like morphology could be evidenced for the G_{12}-*b*-Dex_{51} composition, in line with the larger size of the dextran blocks.

The *in situ* combination of SANS with DLS using a new dialysis set-up proved to be particularly useful for studying such systems.[43] The formation of micellar nanogels is associated to a critical ion concentration (CIC) required to induce G-block multimerization, leading to block copolymer self-assembly. The CIC is therefore the equivalent of the Critical Micelle Concentration (CMC) used for amphiphilic systems. However, as with any chemical equilibrium, a minimum polymer concentration is also required to initiate self-assembly through ionic interactions. Given the high binding constant of G units for divalent ions,[10] this critical concentration is expected to be very low. The CIC was also determined by batch (off-line) measurements combined with light

scattering where calcium was gradually added to the copolysaccharide solution (Figure 5). The addition rate of the calcium solution clearly influences the final state of the micelles. A rapid addition may prompt premature non-equilibrium self-assembly, a phenomenon frequently observed in amphiphilic block copolymers.[57] In the case of slow addition, the characteristics of the micelles are similar to those obtained by the dialysis route (Figure 4).

The main parameter to consider for micelle formation is the block size ratio, which translates the competition between the enthalpy and entropy on the system formation. Increasing the G block size increases the enthalpy interaction with divalent ions in a cooperative process - a minimum of 8 units is required to form stable egg-box junction[64,65] - with the possibility of aggregate formation. Increasing the Dex block size decreases the loss in translational entropy in the micellization process but also increases the loss in conformational entropy due to chain stretching in the corona. Clearly, an optimum block size ratio exists. The G_{12}-*b*-Dex_{51} and G_{19}-*b*-Dex_{45} compositions provided small micelles while the G_{37}-*b*-Dex_{51} copolymer tend to form aggregates in the conditions used, as also observed for the precipitation of G blocks alone in presence of calcium (Figure 5A). In a previous work we also showed that G_{10}-*b*-Dex_{100} only provided loose aggregates.[28] Therefore, a mass fraction of ~20 to ~35% of G is required to obtain well defined micelles whose size then depends on the copolymer's total molar mass. The length of the G blocks also affects the stability of the micelles when subjected to physiological conditions. G_{12}-*b*-Dex_{51} micelles rapidly dissassembled in 150 mM NaCl + 1. 2 mM $CaCl_2$ while G_{19}-*b*-Dex_{45} micelles remained stable for at least 7 days (Figure S14B).

Concerning the role of ion types, it was observed that the size of the block copolysaccharide micelles, as determined by SANS, exhibited a slight decrease with the increase in the affinity the ions for the G-blocks (Ca^{2+} < Sr^{2+} < Ba^{2+}) (Figure 3). As the differences in atomic radius of ions

are negligible (+/- 0.03 nm), the decrease in size should reflect different levels of core compaction according to the egg-box model. Kinetically speaking, the decrease rate of the SLD, probably associated to the dehydration of G blocks followed the affinity order of divalent ions (Figure 3). The nature of the ion exerts a more significant influence on micelle stability than on micelle size, as evidenced by tests conducted in diverse saline media, with strontium and barium giving more stable assemblies (Figure 6C). This was further supported by ion exchange and ligand competition experiments, suggesting that micelles form equilibrium structures rather than frozen aggregates (Figure 7). Such a distinction is important, especially for promoting triggered disassembly in a biological environment.

At the molecular scale, the interaction mechanism leading to micelle formation can be explained in terms of the egg-box model widely used in the case of Ca-alginate hydrogels or Ca-alginate fibers.[4,5,8,9] It has been shown that following the primary formation of egg-box dimers, a slow, lateral association of the egg-box dimers occurs through more unspecific interactions, such as water mediated hydrogen bonding and disordered ions.[9] Interestingly, well diffracting crystals have never been obtained with Ca^{2+} and free oligoguluronates, supporting the concept of partly irregular packing. The slow growth of junction zones in alginate gels has been ascribed to the same phenomenon.[66]

The dimeric state may well exist at low Ca^{2+} concentrations at the point where the molecular weight becomes twice that of the starting material (Figure 5B). This appears indeed to occur transiently for the G_{12}-*b*-Dex_{51} system, both by slow titration or by dialysis. A similar behavior was observed by calcium-titration of the free G_{15} oligomer but is such case precipitation occurs (Figure 5A). The latter is in agreement with the observation by Smidsrød, who reported phase separation upon reaction with Ca^{2+} for longer G-blocks (DP_n 50).[5] Nevertheless, for the rapid

stepwise addition of small amounts of $CaCl_2$ into a G_{15} solution, the stoichiometry found by light scattering at the onset of chain association was R = 0.35 (Figure 5A). For G_{12}-*b*-Dex_{51}, the value raised to R = 0.8 suggesting that excess calcium is needed to mediate lateral association of G blocks (Figures 5 A,B), probably due to entropy constraints introduced by dextran blocks. It may also be noted that also the slightly different chain lengths (12 vs 15) are expected to influence the association behavior in the same direction.[67] This is supported by the higher stability in physiological saline of micelles formed with longer G-blocks. Nevertheless, more detailed studies into the role of chain lengths are needed.

The factor limiting the size of the micellar nanogels is ascribed to an optimal thermodynamic state where the loss of entropy of G blocks, the interfacial tension at the core/shell boundary and the repulsion between dextran blocks are minimized, as evidenced in the electrostatic complexation of oppositely charged double hydrophilic block copolymers.[37] For G_m-*b*-Dex_n, an all-or-none association process was evidenced by neutron and light scattering (Figure 3 and Figure 5), which may appear at odds with previously reported association models based on progressive growth of the egg-box dimers[68] or multiple-step Ca^{2+} binding process.[10,69] It may seem our system has a different behavior where initial chain dimerization cannot be temporally separated from particle growth. This does not preclude the initial step being the formation of an egg-box like dimer followed by micellar growth (Figure 1). Also, we do not preclude that the micellar growth mechanism is related to the slow growth of junction zones in calcium alginate gels.[9] Discrepancies found in literature regarding the binding mechanism of calcium to alginate may also be attributed to the mixing conditions used.[10] For a strongly interacting system, such as alginate-calcium (which is exothermic), the mixing time is expected to play a critical role on the final morphology and equilibrium state (Figure 5A). Under such circumstances, applying slow mixing conditions, such

as those obtained by dialysis should be favored to achieve self-assembly close to equilibrium conditions.

CONCLUSION

There are many methods to manipulate alginate materials at the nanoscale but none of them comply with the thermodynamic equilibrium condition, such as that obtained through the principles of self-assembly. Here, we showed that double-hydrophilic block copolysaccharides containing oligoguluronate (G) and dextran (Dex) yield micellar objects with a gelled core in presence of various divalent ions (Ca^{2+}, Sr^{2+}, Ba^{2+}). We referred these structures as micellar nanogels. The process was monitored *in situ* and real-time by DLS and SANS and supplemented by offline LS and DLS experiments. In comparison to self-assembly based on ionic interaction with sodium polyacrylate-based copolymers, the presence of G blocks provides biological properties as well as high affinity and selectivity towards certain divalent ions like calcium. The mass fraction of G in the diblock copolymer governs the size and stability of micelles, with a value between 20% and 35% resulting in small micelles ($r < 8$ nm) with a star-like morphology that can be freeze dried and redispersed in water. The type of ion (Ca^{2+}, Sr^{2+}, Ca^{2+}) has a negligible effect on micelle size, but it has a strong impact on micelle stability in saline conditions, in accordance with the respective affinity of divalent ions with G blocks. The structures obtained are not in a frozen state. On the contrary, they are living structures capable of exchanging ions and disassembling in the presence of chelating agents such as EDTA, which has some importance in the context of biomedical applications. The small sizes of the micellar nanogels (< 20 nm), combined with a high aggregation number (typically 20) provides a high capacity to sequester relevant multivalent ions in the core structure (about 100 sites for Me^{2+}), making them suitable as injectable systems for potential

applications in biomedical applications such as contrast-enhanced magnetic resonance imaging or radionuclide therapy. The intrinsic biocompatibility of the polysaccharide blocks is also considered as an attractive property in this context.

ASSOCIATED CONTENT

The Supporting Information is available free of charge at https://pubs.acs.org/...

- Chemical characterization of G_m-*b*-Dex_n copolysaccharides and their precursors
- Dialysis setup for DLS and SANS analysis
- Time-resolved DLS and SANS data
- Scattering length density (SLD) values
- Static light scattering data
- Stability of G_m-*b*-Dex_n micelles in saline conditions

AUTHOR INFORMATION

Corresponding Authors

Bjørn E. Christensen - NOBIPOL, Department of Biotechnology and Food Science, NTNU Norwegian University of Science and Technology, Sem Sælands vei 6/8, NO-7491 Trondheim, Norway; E-mail: bjorn.e.christensen@ntnu.no

Christophe Schatz − Université de Bordeaux, CNRS, Bordeaux INP, Laboratoire de chimie des polymères organiques (LCPO), UMR 5629, F-33600 Pessac, France; E-mail : schatz@enscbp.fr

Authors

Martin Fauquignon - Université de Bordeaux, CNRS, Bordeaux INP, Laboratoire de chimie des polymères organiques (LCPO), UMR 5629, F-33600 Pessac, France

Amalie Solberg - NOBIPOL, Department of Biotechnology and Food Science, NTNU Norwegian University of Science and Technology, Sem Sælands vei 6/8, NO-7491 Trondheim, Norway

Lionel Porcar - Institut Laue-Langevin (ILL), F-38042, Grenoble, France

Jean Paul Chapel - Centre de Recherche Paul Pascal (CRPP), UMR CNRS 5031, Université de Bordeaux, F-33600 Pessac, France

Funding Sources

This work was supported by the French National Research Agency (ANR), under Grant ANR 18-CE06-0016 (SISAL Project).

Notes

The authors declare no competing financial interest.

REFERENCES

(1) *Polysaccharide-Based Biomaterials: Delivery of Therapeutics and Biomedical Applications*; Jana, S., Jana, S., Domb, A. J., Eds.; The Royal Society of Chemistry, 2022. https://doi.org/10.1039/9781839166235.
(2) Lee, K. Y.; Mooney, D. J. Alginate: Properties and Biomedical Applications. *Prog. Polym. Sci.* **2012**, *37* (1), 106–126. https://doi.org/10.1016/j.progpolymsci.2011.06.003.
(3) Ebara, M. Carbohydrate-Derived Hydrogels and Microgels; 2010; pp 337–353. https://doi.org/10.1002/9780470944349.ch9.
(4) Donati, I.; Paoletti, S. Material Properties of Alginates. In *Alginates: Biology and Applications*; Rehm, B. H. A., Ed.; Springer Berlin Heidelberg: Berlin, Heidelberg, 2009; pp 1–53. https://doi.org/10.1007/978-3-540-92679-5_1.
(5) Smidsrød, O. Molecular Basis for Some Physical Properties of Alginates in the Gel State. *Faraday Discuss. Chem. Soc.* **1974**, *57* (0), 263–274. https://doi.org/10.1039/DC9745700263.
(6) Solberg, A.; Draget, K. I.; Schatz, C.; Christensen, B. E. Alginate Blocks and Block Polysaccharides: A Review. *Macromol. Symp.* **2023**, *408* (1). https://doi.org/10.1002/masy.202200072.
(7) Draget, K. J.; Moe, S. T.; Skjåk-Bræk, G.; Smidsrød, O. Alginates. In *Food Polysaccharides and Their Applications*; Marcel Dekker, Inc.: New York, NY, USA, 1995; pp 245–286.
(8) Grant, G. T.; Morris, E. R.; Rees, D. A.; Smith, P. J. C.; Thom, D. Biological Interactions between Polysaccharides and Divalent Cations: The Egg-Box Model. *FEBS Lett.* **1973**, *32* (1), 195–198. https://doi.org/10.1016/0014-5793(73)80770-7.

(9) Sikorski, P.; Mo, F.; Skjåk-Bræk, G.; Stokke, B. T. Evidence for Egg-Box-Compatible Interactions in Calcium−Alginate Gels from Fiber X-Ray Diffraction. *Biomacromolecules* **2007**, *8* (7), 2098–2103. https://doi.org/10.1021/bm0701503.

(10) Fang, Y.; Al-Assaf, S.; Phillips, G. O.; Nishinari, K.; Funami, T.; Williams, P. A.; Li, L. Multiple Steps and Critical Behaviors of the Binding of Calcium to Alginate. *J. Phys. Chem. B* **2007**, *111* (10), 2456–2462. https://doi.org/10.1021/jp0689870.

(11) Paques, J. P.; van der Linden, E.; van Rijn, C. J. M.; Sagis, L. M. C. Preparation Methods of Alginate Nanoparticles. *Adv. Colloid Interface Sci.* **2014**, *209*, 163–171. https://doi.org/10.1016/j.cis.2014.03.009.

(12) Merino, S.; Martín, C.; Kostarelos, K.; Prato, M.; Vázquez, E. Nanocomposite Hydrogels: 3D Polymer–Nanoparticle Synergies for On-Demand Drug Delivery. *ACS Nano* **2015**, *9* (5), 4686–4697. https://doi.org/10.1021/acsnano.5b01433.

(13) Salvati, B.; Santagapita, P.; Perullini, M. Exploring the Conditions to Generate Alginate Nanogels. *J. Sol-Gel Sci. Technol.* **2022**, *102* (1), 142–150. https://doi.org/10.1007/s10971-021-05631-w.

(14) Zazzali, I.; Aguirre Calvo, T. R.; Pizones Ruíz-Henestrosa, V. M.; Santagapita, P. R.; Perullini, M. Effects of PH, Extrusion Tip Size and Storage Protocol on the Structural Properties of Ca(II)-Alginate Beads. *Carbohydr. Polym.* **2019**, *206*, 749–756. https://doi.org/10.1016/j.carbpol.2018.11.051.

(15) You, J.-O.; Peng, C.-A. Calcium-Alginate Nanoparticles Formed by Reverse Microemulsion as Gene Carriers. *Macromol. Symp.* **2005**, *219* (1), 147–153. https://doi.org/10.1002/masy.200550113.

(16) Saxena, A.; Sharda, S.; Kumar, S.; Kumar, B.; Shirodkar, S.; Dahiya, P.; Sahney, R. Synthesis of Alginate Nanogels with Polyvalent 3D Transition Metal Cations: Applications in Urease Immobilization. *Polymers* **2022**, *14* (7). https://doi.org/10.3390/polym14071277.

(17) Rondeau, E.; Cooper-White, J. J. Biopolymer Microparticle and Nanoparticle Formation within a Microfluidic Device. *Langmuir* **2008**, *24* (13), 6937–6945. https://doi.org/10.1021/la703339u.

(18) Bazban-Shotorbani, S.; Dashtimoghadam, E.; Karkhaneh, A.; Hasani-Sadrabadi, M. M.; Jacob, K. I. Microfluidic Directed Synthesis of Alginate Nanogels with Tunable Pore Size for Efficient Protein Delivery. *Langmuir* **2016**, *32* (19), 4996–5003. https://doi.org/10.1021/acs.langmuir.5b04645.

(19) Velasco, D.; Tumarkin, E.; Kumacheva, E. Microfluidic Encapsulation of Cells in Polymer Microgels. *Small* **2012**, *8* (11), 1633–1642. https://doi.org/10.1002/smll.201102464.

(20) Mountrichas, G.; Pispas, S. Current Developments in Double Hydrophilic Block Copolymers. In *Polymer Aging, Stabilizers and Amphiphilic Block Copolymers*; 2010; pp 291–326.

(21) Gineste, S.; Mingotaud, C. Double-Hydrophilic Block Copolymer–Metal Ion Associations: Structures, Properties and Applications. *Adv. Colloid Interface Sci.* **2023**, *311*, 102808. https://doi.org/10.1016/j.cis.2022.102808.

(22) Schatz, C.; Lecommandoux, S. Polysaccharide-Containing Block Copolymers: Synthesis, Properties and Applications of an Emerging Family of Glycoconjugates. *Macromol. Rapid Commun.* **2010**, *31* (19), 1664–1684. https://doi.org/10.1002/marc.201000267.

(23) Volokhova, A. S.; Edgar, K. J.; Matson, J. B. Polysaccharide-Containing Block Copolymers: Synthesis and Applications. *Mater. Chem. Front.* **2020**, *4* (1), 99–112. https://doi.org/10.1039/C9QM00481E.

(24) Solberg, A.; Mo, I. V.; Omtvedt, L. Aa.; Strand, B. L.; Aachmann, F. L.; Schatz, C.; Christensen, B. E. Click Chemistry for Block Polysaccharides with Dihydrazide and Dioxyamine Linkers - A Review. *Carbohydr. Polym.* **2022**, *278*, 118840. https://doi.org/10.1016/j.carbpol.2021.118840.

(25) Vikøren Mo, I.; Feng, Y.; Øksnes Dalheim, M.; Solberg, A.; Aachmann, F. L.; Schatz, C.; Christensen, B. E. Activation of Enzymatically Produced Chitooligosaccharides by Dioxyamines and Dihydrazides. *Carbohydr. Polym.* **2020**, *232*, 115748. https://doi.org/10.1016/j.carbpol.2019.115748.

(26) Mo, I. V.; Dalheim, M. Ø.; Aachmann, F. L.; Schatz, C.; Christensen, B. E. 2,5-Anhydro-d-Mannose End-Functionalized Chitin Oligomers Activated by Dioxyamines or Dihydrazides as Precursors of Diblock Oligosaccharides. *Biomacromolecules* **2020**, *21* (7), 2884–2895. https://doi.org/10.1021/acs.biomac.0c00620.

(27) Coudurier, M.; Faivre, J.; Crépet, A.; Ladavière, C.; Delair, T.; Schatz, C.; Trombotto, S. Reducing-End Functionalization of 2,5-Anhydro-d-Mannofuranose-Linked Chitooligosaccharides by Dioxyamine: Synthesis and Characterization. *Molecules* **2020**, *25* (5). https://doi.org/10.3390/molecules25051143.

(28) Solberg, A.; Mo, I. V.; Aachmann, F. L.; Schatz, C.; Christensen, B. E. Alginate-Based Diblock Polymers: Preparation, Characterization and Ca-Induced Self-Assembly. *Polym. Chem.* **2021**, *12* (38), 5412–5425. https://doi.org/10.1039/D1PY00727K.

(29) Courtecuisse, E.; Bourasseau, S.; Christensen, B. E.; Schatz, C. Synthesis of Linear Chitosan-Block-Dextran Copolysaccharides with Dihydrazide and Dioxyamine Linkers. *Carbohydr. Polym.* **2024**, *345*, 122576. https://doi.org/10.1016/j.carbpol.2024.122576.

(30) Sondjaja, H. R.; Hatton, T. A.; Tam, K. C. Self-Assembly of Poly(Ethylene Oxide)-Block-Poly(Acrylic Acid) Induced by CaCl2: Mechanistic Study. *Langmuir* **2008**, *24* (16), 8501–8506. https://doi.org/10.1021/la800727e.

(31) Li, Y.; Gong, Y.-K.; Nakashima, K.; Murata, Y. Nanoaggregate Formation of Poly(Ethylene Oxide)-b-Polymethacrylate Copolymer Induced by Alkaline Earth Metal Ion Binding. *Langmuir* **2002**, *18* (18), 6727–6729. https://doi.org/10.1021/la025811q.

(32) Bronich, T. K.; Keifer, P. A.; Shlyakhtenko, L. S.; Kabanov, A. V. Polymer Micelle with Cross-Linked Ionic Core. *J. Am. Chem. Soc.* **2005**, *127* (23), 8236–8237. https://doi.org/10.1021/ja043042m.

(33) Carl, N.; Prévost, S.; Schweins, R.; Huber, K. Ion-Selective Binding as a New Trigger for Micellization of Block Copolyelectrolytes with Two Anionic Blocks. *Soft Matter* **2019**, *15* (41), 8266–8271. https://doi.org/10.1039/C9SM01138B.

(34) Gérardin, C.; Sanson, N.; Bouyer, F.; Fajula, F.; Putaux, J.-L.; Joanicot, M.; Chopin, T. Highly Stable Metal Hydrous Oxide Colloids by Inorganic Polycondensation in Suspension. *Angew. Chem. Int. Ed.* **2003**, *42* (31), 3681–3685. https://doi.org/10.1002/anie.200350917.

(35) Banerjee, A.; Bandopadhyay, R. Use of Dextran Nanoparticle: A Paradigm Shift in Bacterial Exopolysaccharide Based Biomedical Applications. *Int. J. Biol. Macromol.* **2016**, *87*, 295–301. https://doi.org/10.1016/j.ijbiomac.2016.02.059.

(36) Yu, M.; Huang, S.; Yu, K. J.; Clyne, A. M. Dextran and Polymer Polyethylene Glycol (PEG) Coating Reduce Both 5 and 30 Nm Iron Oxide Nanoparticle Cytotoxicity in 2D and 3D Cell Culture. *Int. J. Mol. Sci.* **2012**, *13* (5), 5554–5570. https://doi.org/10.3390/ijms13055554.

(37) Harada, A.; Kataoka, K. Chain Length Recognition: Core-Shell Supramolecular Assembly from Oppositely Charged Block Copolymers. *Science* **1999**, *283* (5398), 65–67. https://doi.org/10.1126/science.283.5398.65.

(38) Nicolai, T.; Colombani, O.; Chassenieux, C. Dynamic Polymeric Micelles versus Frozen Nanoparticles Formed by Block Copolymers. *Soft Matter* **2010**, *6* (14), 3111–3118. https://doi.org/10.1039/B925666K.
(39) Hayward, R. C.; Pochan, D. J. Tailored Assemblies of Block Copolymers in Solution: It Is All about the Process. *Macromolecules* **2010**, *43* (8), 3577–3584. https://doi.org/10.1021/ma9026806.
(40) Jain, S.; Bates, F. S. Consequences of Nonergodicity in Aqueous Binary PEO−PB Micellar Dispersions. *Macromolecules* **2004**, *37* (4), 1511–1523. https://doi.org/10.1021/ma035467j.
(41) Denkova, A. G.; Mendes, E.; Coppens, M.-O. Non-Equilibrium Dynamics of Block Copolymer Micelles in Solution: Recent Insights and Open Questions. *Soft Matter* **2010**, *6* (11), 2351–2357. https://doi.org/10.1039/C001175B.
(42) Nagarajan, R. "Non-Equilibrium" Block Copolymer Micelles with Glassy Cores: A Predictive Approach Based on Theory of Equilibrium Micelles. *Liq. Films Interfaces Colloidal Dispers.* **2015**, *449*, 416–427. https://doi.org/10.1016/j.jcis.2014.12.077.
(43) Fauquignon, M.; Porcar, L.; Brûlet, A.; Le Meins, J.-F.; Sandre, O.; Chapel, J.-P.; Schmutz, M.; Schatz, C. In Situ Monitoring of Block Copolymer Self-Assembly via Solvent Exchange through Controlled Dialysis with Light and Neutron Scattering Detection. *ACS Macro Lett.* **2023**, 1272–1279. https://doi.org/10.1021/acsmacrolett.3c00286.
(44) Braccini, I.; Pérez, S. Molecular Basis of Ca2+-Induced Gelation in Alginates and Pectins: The Egg-Box Model Revisited. *Biomacromolecules* **2001**, *2* (4), 1089–1096. https://doi.org/10.1021/bm010008g.
(45) Nordgård, C. T.; Draget, K. I. Oligosaccharides As Modulators of Rheology in Complex Mucous Systems. *Biomacromolecules* **2011**, *12* (8), 3084–3090. https://doi.org/10.1021/bm200727c.
(46) Aarstad, O. A.; Tøndervik, A.; Sletta, H.; Skjåk-Bræk, G. Alginate Sequencing: An Analysis of Block Distribution in Alginates Using Specific Alginate Degrading Enzymes. *Biomacromolecules* **2012**, *13*, 106−116.
(47) Cousin, F. Small Angle Neutron Scattering. *EPJ Web Conf.* **2015**, *104*. https://doi.org/10.1051/epjconf/201510401004.
(48) Guinier, A.; Fournet, G. *Small-Angle Scattering of X-Rays*; John Wiley and Sons: New York, 1955.
(49) Wesslau, V. H. Zur Kenntnis von Acrylsäure Enthaltenden Copolymerdispersionen. I. Über Die Auswertung von Streulichtmessungen. *Makromol. Chem.* **1963**, *69* (1), 213–219. https://doi.org/10.1002/macp.1963.020690117.
(50) Itakura, M.; Shimada, K.; Matsuyama, S.; Saito, T.; Kinugasa, S. A Convenient Method to Determine the Rayleigh Ratio with Uniform Polystyrene Oligomers. *J. Appl. Polym. Sci.* **2006**, *99* (4), 1953–1959. https://doi.org/10.1002/app.22695.
(51) Vena, M. P.; de Moor, D.; Ianiro, A.; Tuinier, R.; Patterson, J. P. Kinetic State Diagrams for a Highly Asymmetric Block Copolymer Assembled in Solution. *Soft Matter* **2021**, *17* (4), 1084–1090. https://doi.org/10.1039/D0SM01596B.
(52) Sedlák, M. What Can Be Seen by Static and Dynamic Light Scattering in Polyelectrolyte Solutions and Mixtures? *Langmuir* **1999**, *15* (12), 4045–4051. https://doi.org/10.1021/la981189j.
(53) Sanson, N.; Bouyer, F.; Destarac, M.; In, M.; Gérardin, C. Hybrid Polyion Complex Micelles Formed from Double Hydrophilic Block Copolymers and Multivalent Metal Ions:

Size Control and Nanostructure. *Langmuir* **2012**, *28* (8), 3773–3782. https://doi.org/10.1021/la204562t.

(54) Vold, I. M. N.; Kristiansen, K. A.; Christensen, B. E. A Study of the Chain Stiffness and Extension of Alginates, in Vitro Epimerized Alginates, and Periodate-Oxidized Alginates Using Size-Exclusion Chromatography Combined with Light Scattering and Viscosity Detectors. *Biomacromolecules* **2006**, *7* (7), 2136–2146. https://doi.org/10.1021/bm060099n.

(55) Burchard, W. Static and Dynamic Light Scattering from Branched Polymers and Biopolymers. In *Light Scattering from Polymers*; Springer Berlin Heidelberg: Berlin, Heidelberg, 1983; pp 1–124.

(56) MYKLESTAD, S.; HAUG, A. STUDIES ON THE SOLUBILITY OF ALGINIC ACID FROM ASCOPHYLLUM NODOSUM AT LOW PH. In *Proceedings of the Fifth International Seaweed Symposium, Halifax, August 25–28, 1965*; YOUNG, E. G., McLACHLAN, J. L., Eds.; Pergamon, 1966; pp 297–303. https://doi.org/10.1016/B978-0-08-011841-3.50048-3.

(57) Johnson, B. K.; Prud'homme, R. K. Mechanism for Rapid Self-Assembly of Block Copolymer Nanoparticles. *Phys. Rev. Lett.* **2003**, *91* (11), 118302. https://doi.org/10.1103/PhysRevLett.91.118302.

(58) Mørch, Ý. A.; Donati, I.; Strand, B. L.; Skjåk-Bræk, G. Effect of Ca2+, Ba2+, and Sr2+ on Alginate Microbeads. *Biomacromolecules* **2006**, *7* (5), 1471–1480. https://doi.org/10.1021/bm060010d.

(59) Bassett, D. C.; Håti, A. G.; Melø, T. B.; Stokke, B. T.; Sikorski, P. Competitive Ligand Exchange of Crosslinking Ions for Ionotropic Hydrogel Formation. *J. Mater. Chem. B* **2016**, *4* (37), 6175–6182. https://doi.org/10.1039/C6TB01812B.

(60) Atkins, E. D. T.; Nieduszynski, I. A.; Mackie, W.; Parker, K. D.; Smolko, E. E. Structural Components of Alginic Acid. II. The Crystalline Structure of Poly-α-L-Guluronic Acid. Results of X-Ray Diffraction and Polarized Infrared Studies. *Biopolymers* **1973**, *12* (8), 1879–1887. https://doi.org/10.1002/bip.1973.360120814.

(61) Sinn, C. G.; Dimova, R.; Antonietti, M. Isothermal Titration Calorimetry of the Polyelectrolyte/Water Interaction and Binding of Ca2+: Effects Determining the Quality of Polymeric Scale Inhibitors. *Macromolecules* **2004**, *37* (9), 3444–3450. https://doi.org/10.1021/ma030550s.

(62) Carl, N.; Prévost, S.; Schweins, R.; Huber, K. Contrast Variation of Micelles Composed of Ca2+ and Block Copolymers of Two Negatively Charged Polyelectrolytes. *Colloid Polym. Sci.* **2020**, *298* (7), 663–679. https://doi.org/10.1007/s00396-019-04596-1.

(63) Nyrkova, I. A.; Semenov, A. N. Multimerization: Closed or Open Association Scenario? *Eur. Phys. J. E* **2005**, *17* (3), 327–337. https://doi.org/10.1140/epje/i2004-10146-5.

(64) Stokke, B. T.; Smidsroed, O.; Bruheim, P.; Skjaak-Braek, G. Distribution of Uronate Residues in Alginate Chains in Relation to Alginate Gelling Properties. *Macromolecules* **1991**, *24* (16), 4637–4645. https://doi.org/10.1021/ma00016a026.

(65) Stokke, B. T.; Smidsrød, O.; Zanetti, F.; Strand, W.; Skjåk-Bræk, G. Distribution of Uronate Residues in Alginate Chains in Relation to Alginate Gelling Properties — 2: Enrichment of β-d-Mannuronic Acid and Depletion of α-l-Guluronic Acid in Sol Fraction. *Carbohydr. Polym.* **1993**, *21* (1), 39–46. https://doi.org/10.1016/0144-8617(93)90115-K.

(66) Yuguchi, Y.; Hasegawa, A.; Padoł, A. M.; Draget, K. I.; Stokke, B. T. Local Structure of Ca2+ Induced Hydrogels of Alginate–Oligoguluronate Blends Determined by Small-Angle-

X-Ray Scattering. *Carbohydr. Polym.* **2016**, *152*, 532–540. https://doi.org/10.1016/j.carbpol.2016.07.020.

(67) Kohn, Rudolf; Larsen, B. Preparation of Water-Soluble Polyuronic Acids and Their Calcium Salts, and the Determination of Calcium Ion Activity in Relation to the Degree of Polymerization. *Acta Chem. Scand.* **1972**, *26*, 2455–2468. https://doi.org/10.3891/acta.chem.scand.26-2455.

(68) Borgogna, M.; Skjåk-Bræk, G.; Paoletti, S.; Donati, I. On the Initial Binding of Alginate by Calcium Ions. The Tilted Egg-Box Hypothesis. *J. Phys. Chem. B* **2013**, *117* (24), 7277–7282. https://doi.org/10.1021/jp4030766.

(69) Wang, Y.; Zhao, Y.; He, J.; Sun, C.; Lu, W.; Zhang, Y.; Fang, Y. Doubling Growth of Egg-Box Structure during Calcium-Mediated Molecular Assembly of Alginate. *J. Colloid Interface Sci.* **2023**, *634*, 747–756. https://doi.org/10.1016/j.jcis.2022.12.096.

Supporting Information

Micellar Nanogels from Alginate-based Diblock Copolysaccharides

Martin Fauquignon, Amalie Solberg, Lionel Porcar, Jean-Paul Chapel, Bjørn E. Christensen, Christophe Schatz

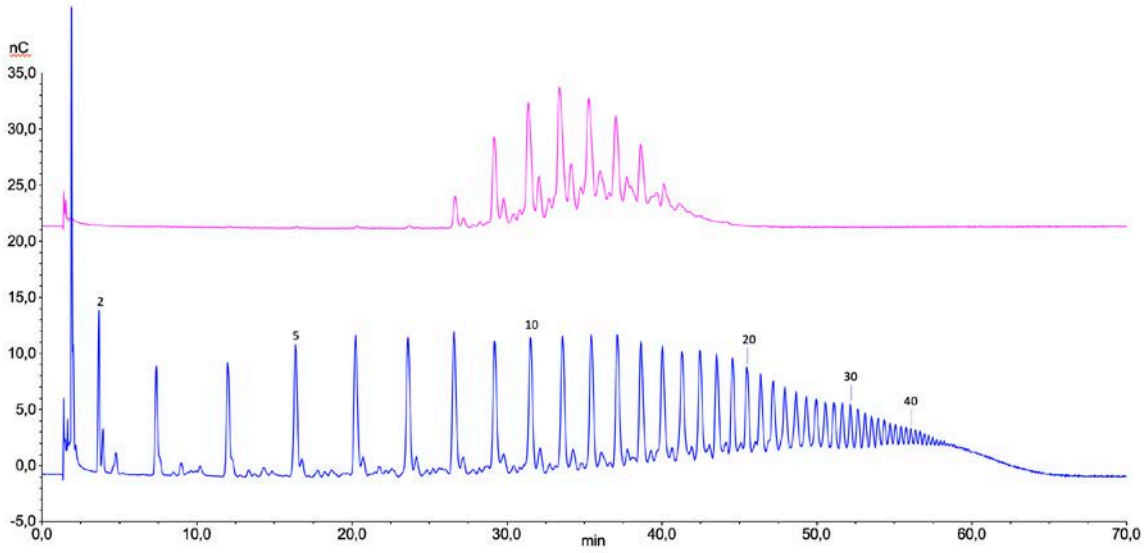

Figure S1a. HPAEC-PAD chromatogram of the G_{12} fraction (top). G-block standards (unfractionated hydrolysate) are included for DP assignment. Peak integration corresponds to DP_n 11.8 (rounded off to 12) and dispersity (DP_w/DP_n) of 1.03

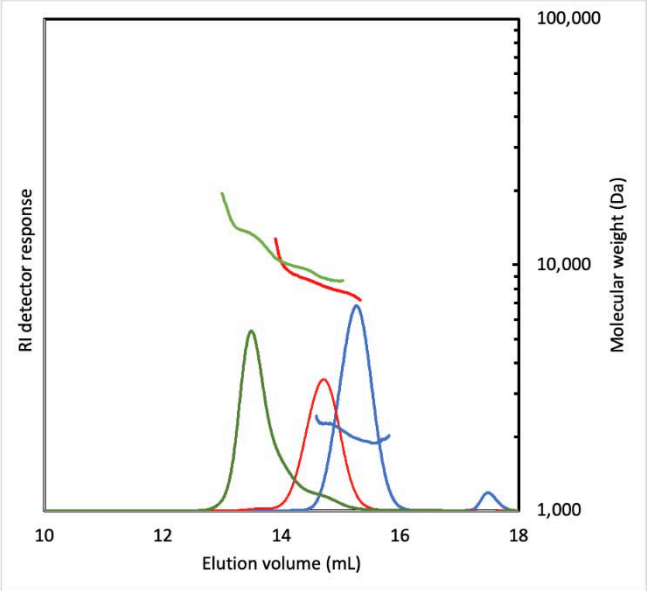

	M_w (kDa)	M_n (kDa)	M_w/M_n
G_{12}	2.0	2.0	1.01
Dex_{51}-PDHA	8.5	8.3	1.02
G_{12}-*b*-Dex_{51}	12.8	12.4	1.03

Figure S1b. SEC-MALS analysis of G_{10} (blue), Dex_{51}-PDHA (red) and G_{12}-*b*-Dex_{51} (green). Columns: TSK G-4000 and G-2500 (serially connected). Eluent: 150 mM NaCl, 10 mM EDTA, pH 6.0.

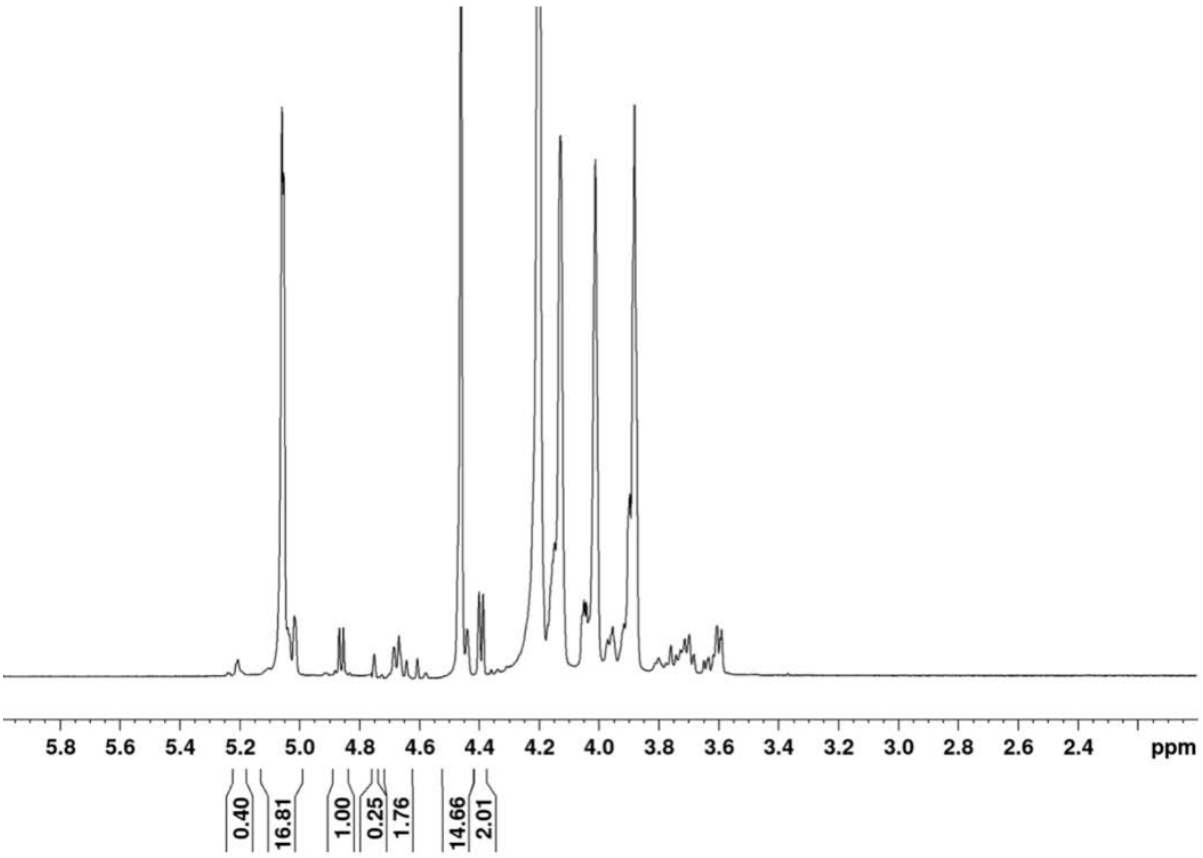

Figure S1c. ^{1}H-NMR spectrum of G_{12}-*b*-Dex_{51} recorded in D_2O at 82°C. Integrals for main peaks based on assignments in the literature:[1] 5.2 ppm: H-1α (red. end), 5.1 ppm: H-1 internal, 4.9 ppm: H-1β (red. end), 4.7 ppm: GGM-5, 4.6-4.7 ppm: (M-1 internal), 4.5 ppm: GG-5). Integrals correspond to F_G = 0.91, DP_n = 14.

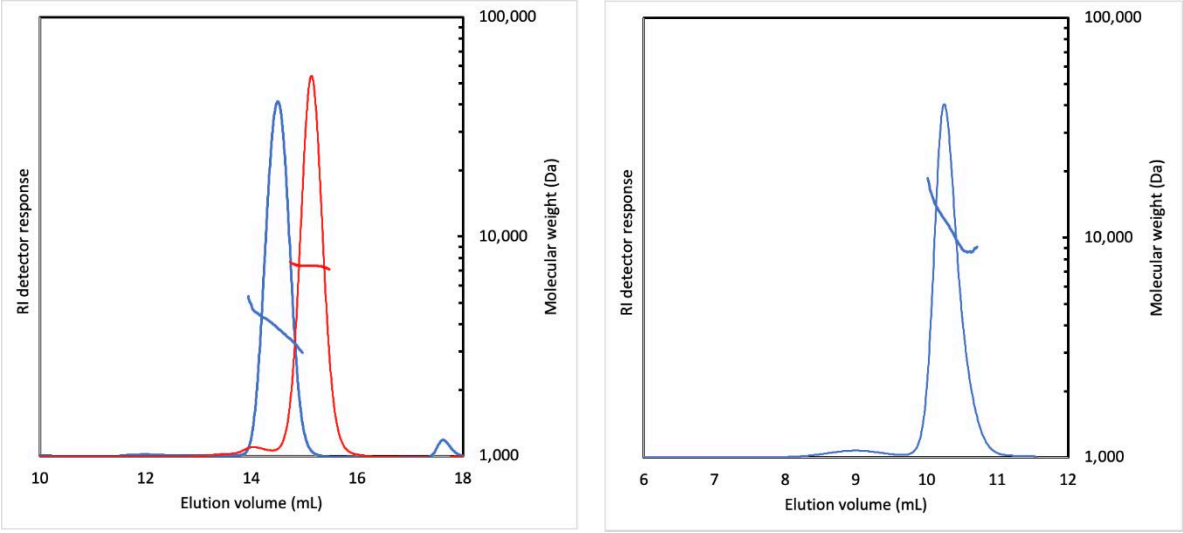

	M_w (kDa)	M_n (kDa)	M_w/M_n
G_{19}	3.83	3.79	1.01
Dex_{45}-PDHA	7.36	7.36	1.00
G_{19}-*b*-Dex_{45}	11.6	11.1	1.04

Figure S2a. Left: SEC-MALS analysis of G_{19} and Dex_{45}-PDHA.Column: TSK G-4000 and G-2500 (serially connected). Eluent: 150 mM NaCl, 10 mM EDTA, pH 6.0. Right: SEC-MALS of G_{19}-*b*-Dex_{45}. Column: OHpak LB-806M. Eluent: 1.2 mM $CaCl_2$, 150 mM NaCl, pH 6.0.

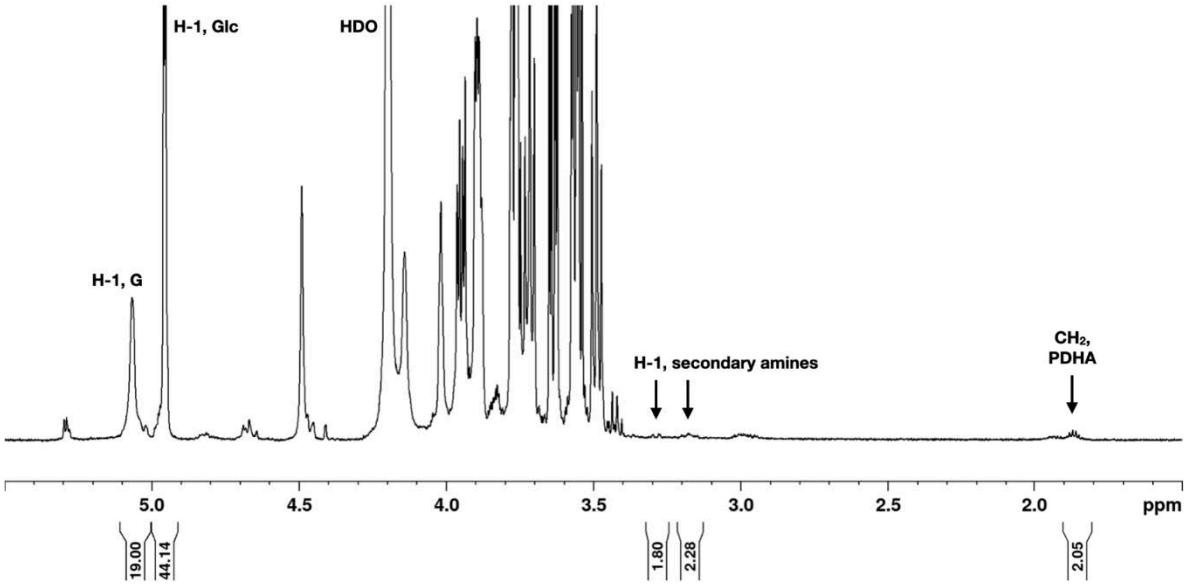

Figure S2b. ^{1}H-NMR spectrum of G_{19}-*b*-Dex_{45} recorded in D_2O at 82°C. Assignments for main peaks shown in the figure are based on the literature.[1]

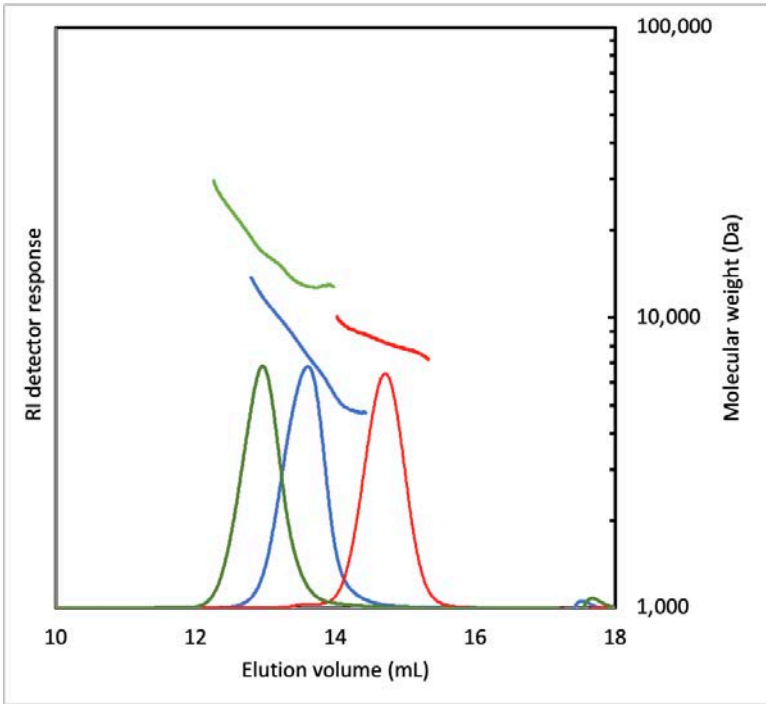

	M_w (kDa)	M_n (kDa)	M_w/M_n
G_{37}	7.9	7.5	1.06
Dex_{51}-PDHA	8.5	8.3	1.02
G_{37}-*b*-Dex_{51}	17.7	17.0	1.04

Figure S3. SEC-MALS analysis of G_{37} (blue), Dex_{51}-PDHA (red) and G_{37}-*b*-Dex_{51} (green). Column: TSK G-4000 and G-2500 (serially connected). Eluent: 150 mM NaCl, 10 mM EDTA, pH 6.0.

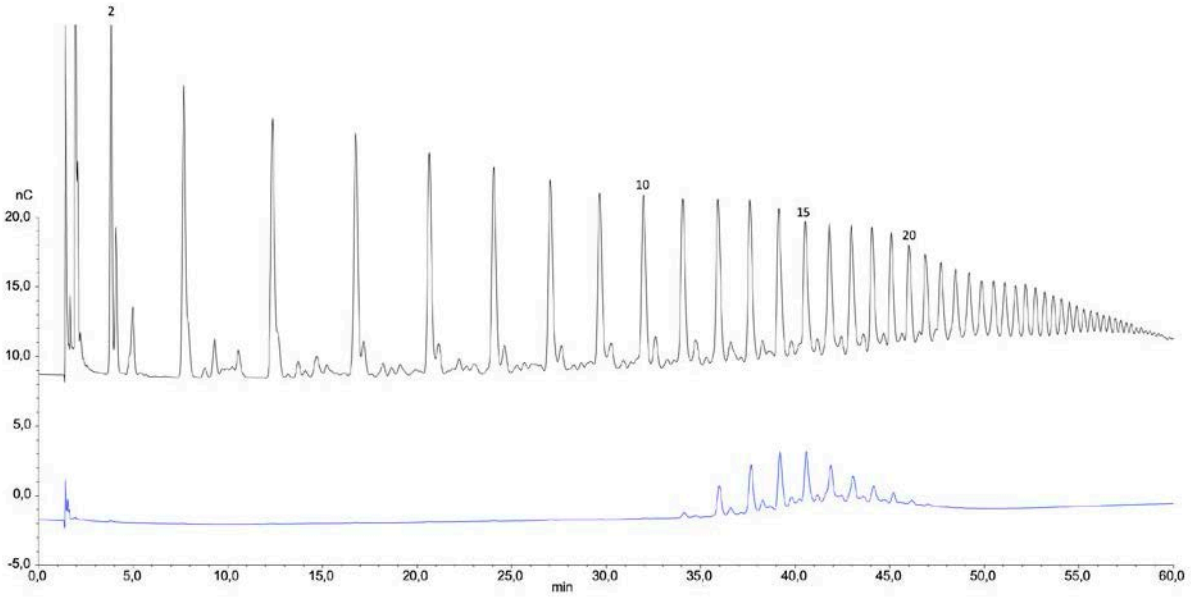

Figure S4. HPAEC-PAD chromatogram of the G_{15} fraction (bottom). G-block standards (unfractionated hydrolysate) are included for DP assignment. Peak integration corresponds to DP_n 15 and dispersity (M_w/M_n) of 1.02.

.

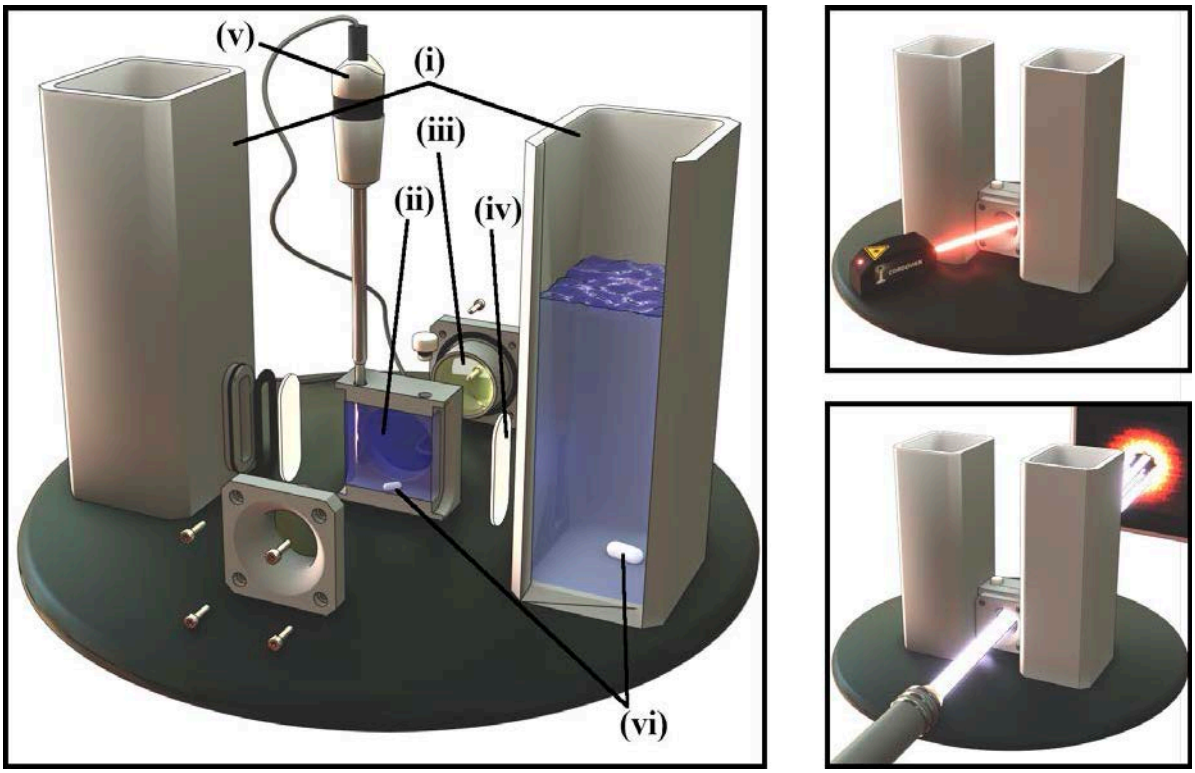

Figure S5. (left) Exploded view of the dialysis setup used for continuous kinetic monitoring of alginate micellar nanogels. The main components are: i) 2 lateral reservoirs containing the solution of divalent ions (2 × 250 mL); ii) Scattering cell containing the G_m-*b*-Dex_m solution in D_2O (V = 4.5 mL); iii) Quartz windows (thickness = 1 or 2 mm); iv) Custom-cut ultrafiltration discs in regenerated cellulose of defined porosity (×2); v) Conductivity probe, vi) Reservoir and cell stirring. All plastic parts are made in solvent-resistant PEEK. (right) Configuration of the remote DLS head and SANS detection. More details can be found in Ref.[2]

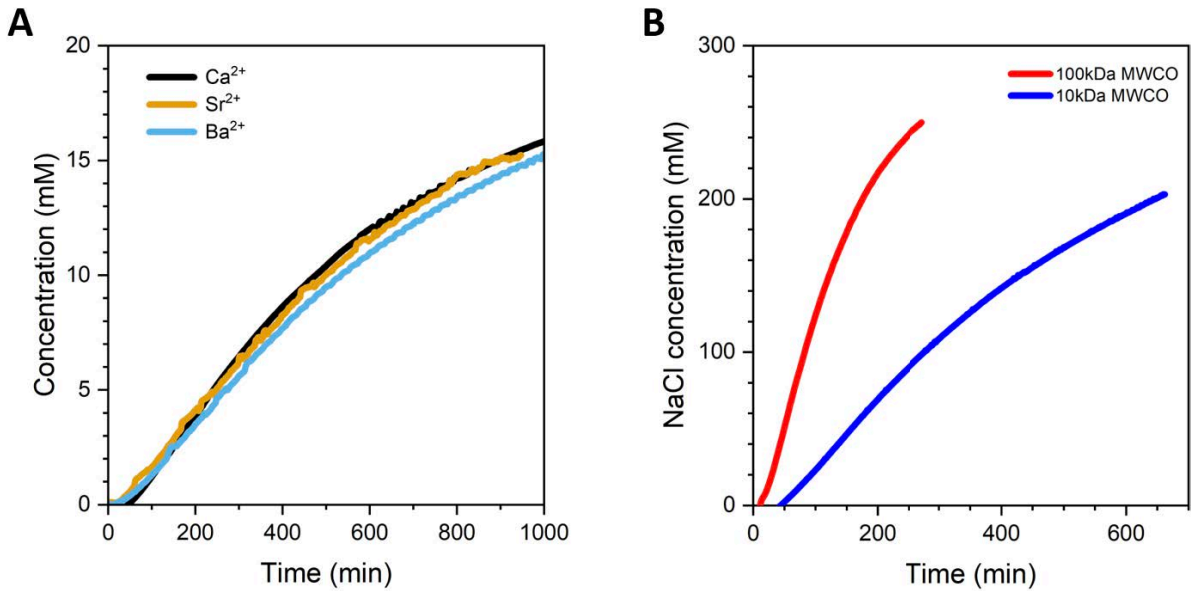

Figure S6. Time variation of the ion concentration in the dialysis cell determined from conductivity measurements. A) 4.5 ml of a 10 mM NaCl solution was dialyzed against 2 x 100 ml of 10 mM NaCl with either 20 mM $CaCl_2$, 20 mM $SrCl_2$ or 20 mM $BaCl_2$ by using a dialysis membrane with a MWCO of 10 kDa. B) 4.5 ml of pure water was dialyzed against 2 x 100 ml of 300 mM NaCl solution with a membrane MWCO of 10 kDa and 100kDa. The conductivities of $CaCl_2$, $SrCl_2$, $BaCl_2$ and NaCl solutions at various concentrations were determined prior to dialysis experiments.

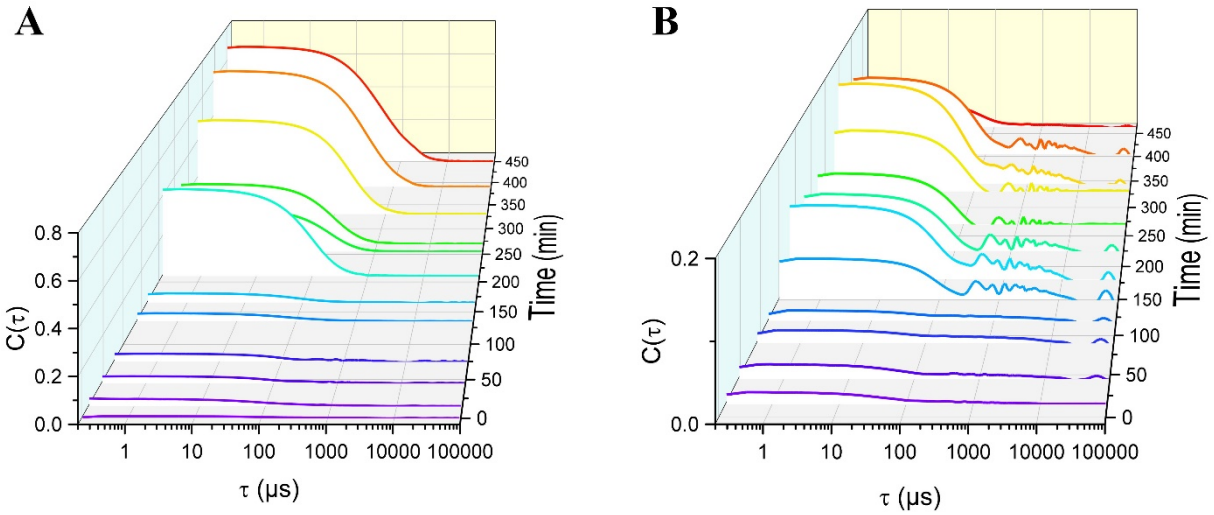

Figure S7. Time-resolved DLS monitoring of the dialysis of G_m-*b*-Dex_n against calcium ion solution for two block copolysaccharide compositions: A) G_{37}-*b*-Dex_{51}. B) G_{12}-*b*-Dex_{51}. Correlation functions are plotted at different dialysis times. Copolymer were dissolved at 4 $g.L^{-1}$ in 10 mM NaCl. The dialysis was performed against 2 x 100 mL of 20 mM $CaCl_2$ in 10 mM NaCl using a dialysis membrane with a MWCO of 10 kDa.

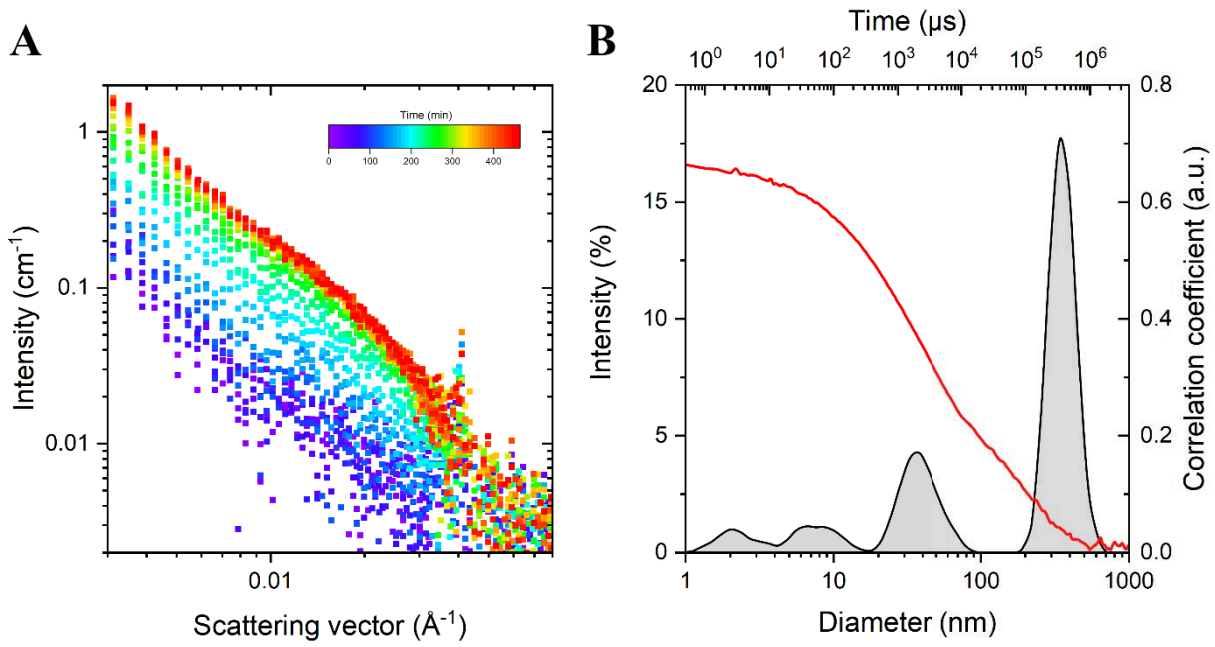

Figure S8. A) Time-resolved SANS monitoring of the dialysis self-assembly of G_{37}-*b*-Dex_{51} at 4 g/L in 10 mM NaCl against 20 mM $CaCl_2$ + 10 mM NaCl using a dialysis membrane with MWCO of 10 kDa. B) Size distribution and correlation curve of G_{37}-*b*-Dex_{51}/Ca nanoparticles as determined by DLS after dialysis of the copolysaccharide against $CaCl_2$.

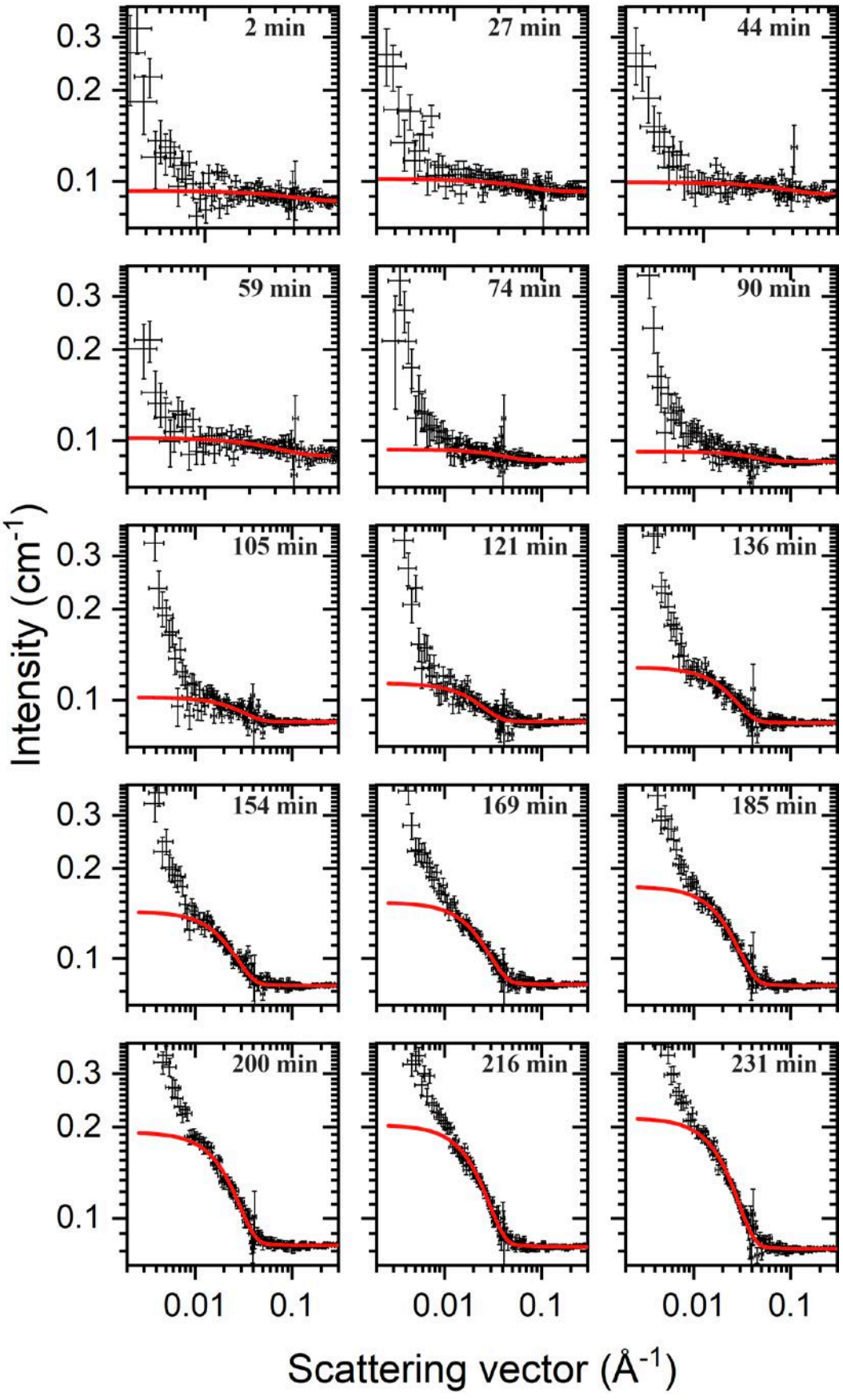
2 min
27 min
44 min
59 min
74 min
90 min
105 min
121 min
136 min
154 min
169 min
185 min
200 min
216 min
231 min
0.3
0.2
0.1
0.01
0.1
Intensity (cm-1)
Scattering vector (Å-1)

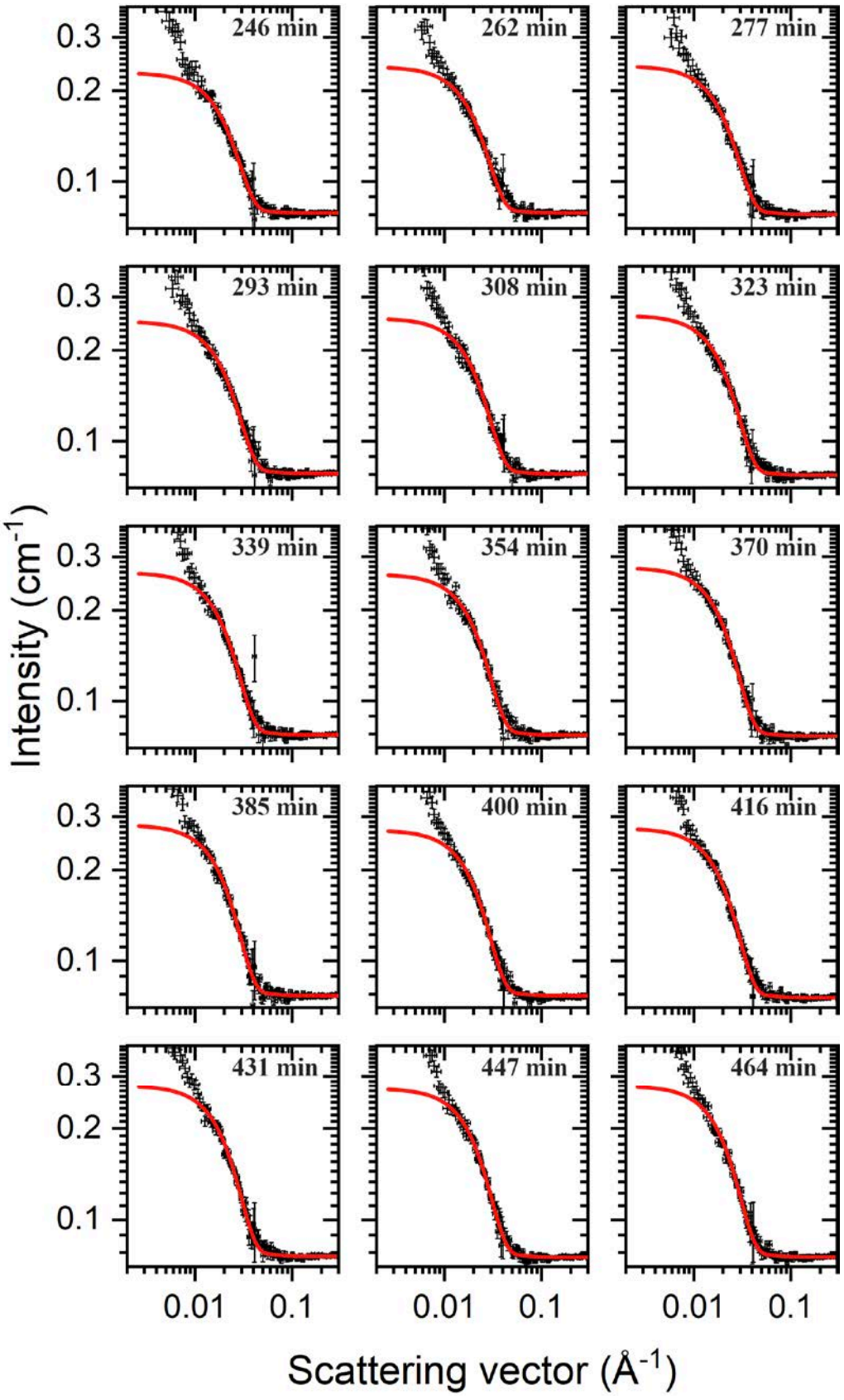

Figure S9. Time-resolved SANS monitoring of the dialysis self-assembly of G_{12}-*b*-Dex_{51} in presence of Ca^{2+}. Data were fitted using sphere form factor (red line).

Table S1. Parameters used to fit the SANS curves of the dialysis self-assembly of G_{12}-*b*-Dex_{51} in presence of Ca^{2+}. A monodisperse sphere form factor was used.

Time (min)	Scale (imposed)	Background (imposed)	SLD (10^{-6} Å^{-2})	SLD error (10^{-6} Å^{-2})	Solvent SLD (10^{-6} Å^{-2})	Radius (nm)	Radius SD (nm)
3	0.005	0.0860	6.246	0.031	6.4	4.56	0.91
27		0.0924	6.279	0.023		5.91	1.18
44		0.0905	6.239	0.028		4.80	0.96
59		0.0891	6.254	0.019		5.81	1.16
74		0.0861	6.235	0.030		4.41	0.88
90		0.0853	6.221	0.032		4.09	0.82
105		0.0846	6.232	0.016		5.84	1.17
121		0.0847	6.251	0.008		7.50	1.50
136		0.0839	6.194	0.008		6.95	1.39
154		0.0814	6.173	0.006		7.34	1.47
169		0.0820	6.131	0.006		6.87	1.37
185		0.0813	6.103	0.005		7.00	1.40
200		0.0814	6.094	0.005		7.26	1.45
216		0.0807	6.079	0.004		7.28	1.46
231		0.0793	6.069	0.004		7.36	1.47
246		0.0787	6.058	0.004		7.47	1.49
262		0.0788	6.048	0.004		7.50	1.50
277		0.0780	6.037	0.004		7.37	1.47
293		0.0783	6.029	0.004		7.37	1.47
308		0.0780	6.026	0.004		7.43	1.49
323		0.0773	6.020	0.004		7.43	1.49
339		0.0773	6.025	0.003		7.57	1.51
354		0.0771	6.012	0.004		7.36	1.47
370		0.0766	6.014	0.003		7.57	1.51
385		0.0768	6.013	0.003		7.62	1.52
400		0.0768	6.011	0.004		7.46	1.49
416		0.0757	6.008	0.003		7.49	1.50
431		0.0757	6.005	0.003		7.48	1.50
447		0.0752	5.995	0.004		7.29	1.46
464		0.0753	5.997	0.004		7.38	1.48

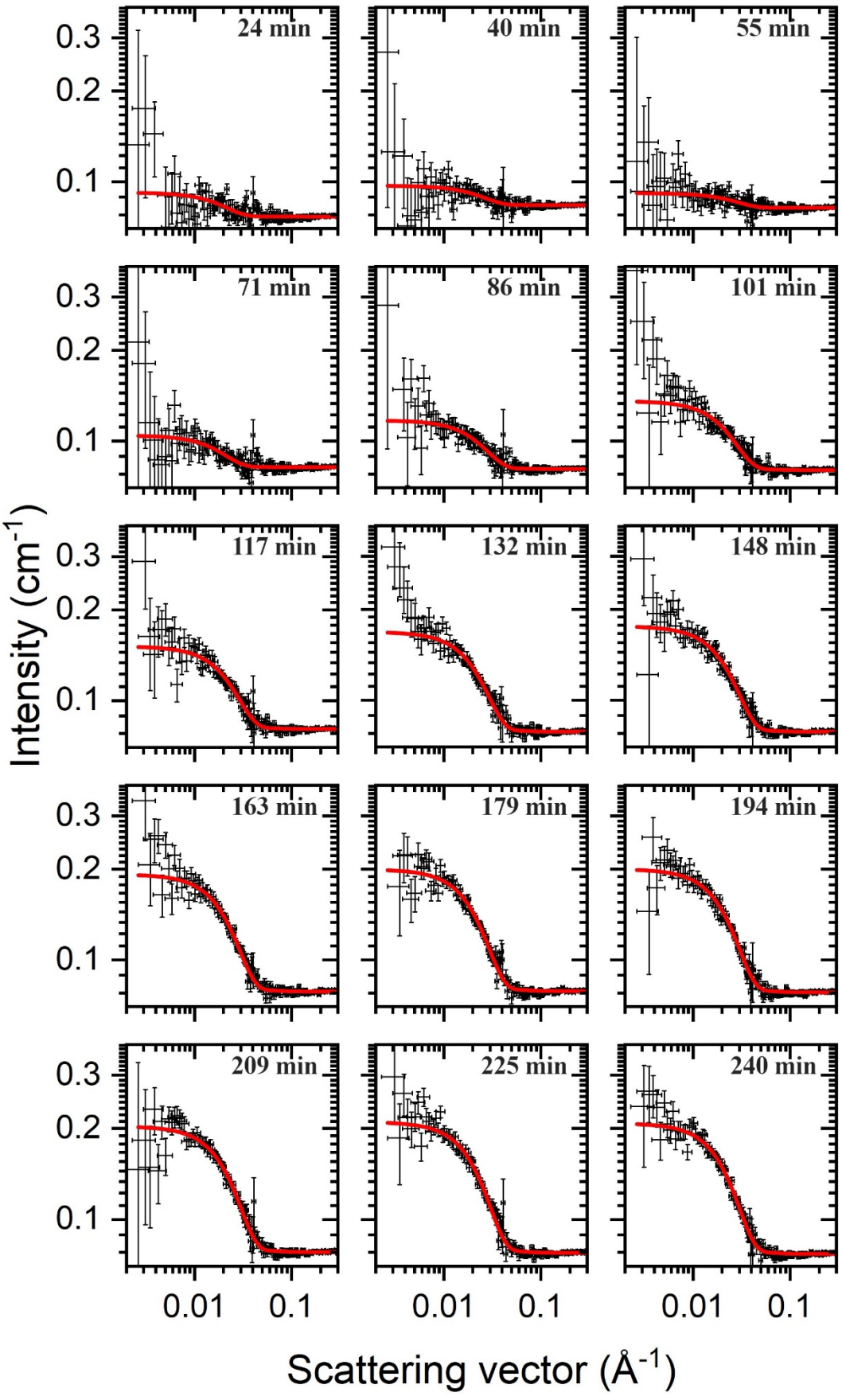
24 min
40 min
55 min
71 min
86 min
101 min
117 min
132 min
148 min
163 min
179 min
194 min
209 min
225 min
240 min
0.3
0.2
0.1
0.01
0.1
Intensity (cm-1)
Scattering vector (Å-1)

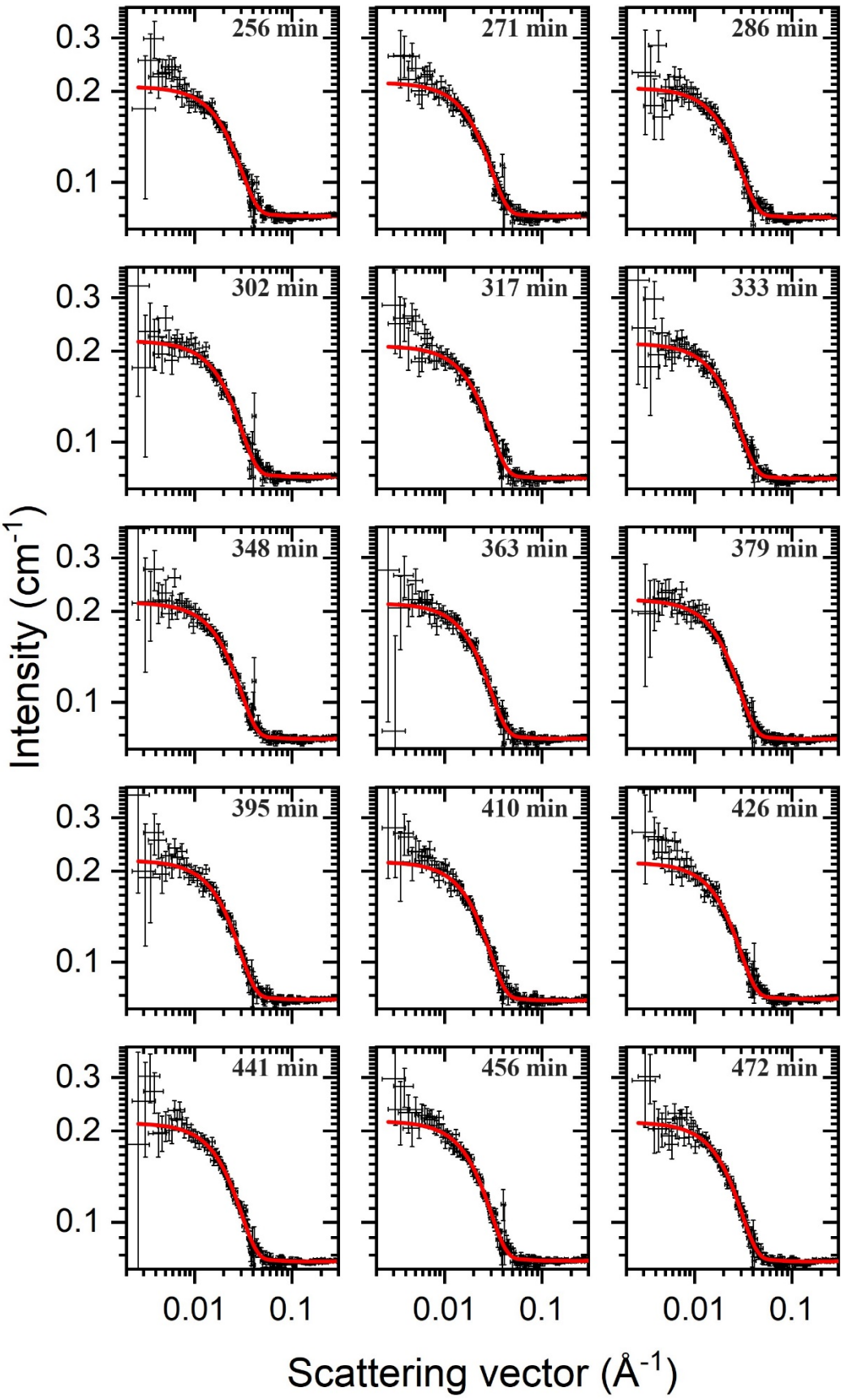

Figure S10. Time-resolved SANS monitoring of the dialysis self-assembly of G_{12}-*b*-Dex_{51} in presence of Sr^{2+}. Data were fitted using sphere form factor (red line).

Table S2. Parameters used to fit the SANS curves of the dialysis self-assembly of G_{12}-*b*-Dex_{51} in presence of Sr^{2+}. A monodisperse sphere form factor was used.

Time (min)	Scale (imposed)	Background (imposed)	SLD (10^{-6} Å^{-2})	SLD error (10^{-6} Å^{-2})	Solvent SLD (10^{-6} Å^{-2})	Radius (nm)	Radius SD (nm)
3	0.005	0.0768	6.312	0.009	6.4	8.66	1.73
24		0.0850	6.301	0.015		7.05	1.41
40		0.0838	6.287	0.013		6.98	1.40
55		0.0821	6.286	0.018		6.25	1.25
71		0.0820	6.299	0.007		8.95	1.79
86		0.0809	6.209	0.008		6.84	1.37
101		0.0803	6.171	0.007		6.99	1.40
117		0.0805	6.138	0.006		6.93	1.39
132		0.0788	6.115	0.005		7.10	1.42
148		0.0788	6.093	0.005		6.93	1.39
163		0.0787	6.085	0.005		7.18	1.44
179		0.0789	6.080	0.004		7.25	1.45
194		0.0782	6.066	0.005		7.06	1.41
209		0.0780	6.061	0.005		7.06	1.41
225		0.0776	6.053	0.004		7.09	1.42
240		0.0769	6.057	0.004		7.13	1.43
256		0.0774	6.050	0.005		7.01	1.40
271		0.0773	6.049	0.004		7.11	1.42
286		0.0767	6.053	0.005		7.01	1.40
302		0.0768	6.046	0.004		7.12	1.42
317		0.0760	6.056	0.004		7.12	1.42
333		0.0758	6.062	0.004		7.28	1.46
348		0.0756	6.054	0.004		7.19	1.44
363		0.0757	6.055	0.004		7.18	1.44
379		0.0754	6.063	0.004		7.41	1.48
395		0.0753	6.061	0.004		7.37	1.47
410		0.0747	6.064	0.004		7.38	1.48
426		0.0756	6.060	0.004		7.28	1.46
441		0.0742	6.049	0.004		7.14	1.43
456		0.0746	6.054	0.004		7.25	1.45

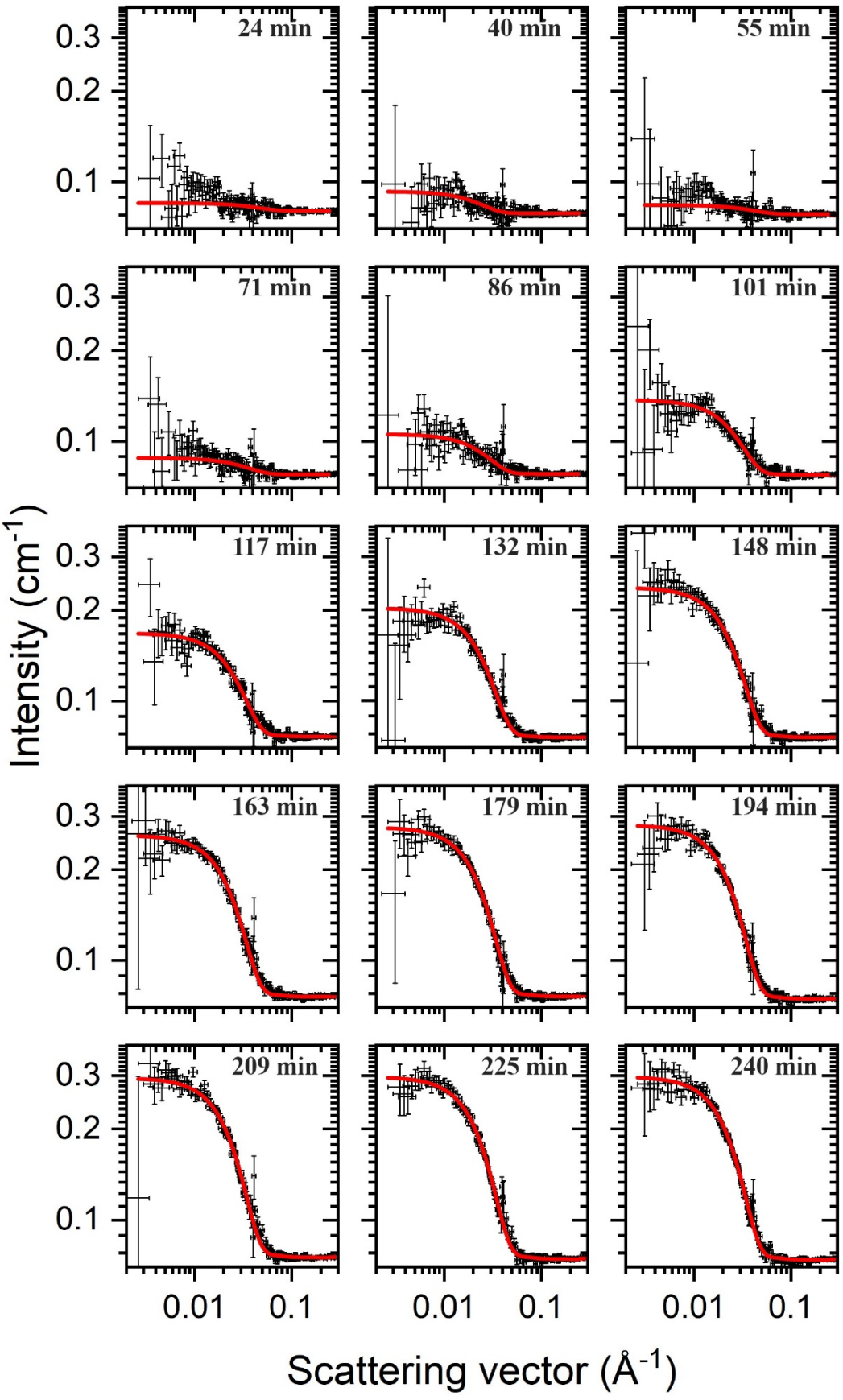
24 min
40 min
55 min
71 min
86 min
101 min
117 min
132 min
148 min
163 min
179 min
194 min
209 min
225 min
240 min
0.3
0.2
0.1
0.01
0.1
Intensity (cm-1)
Scattering vector (Å-1)

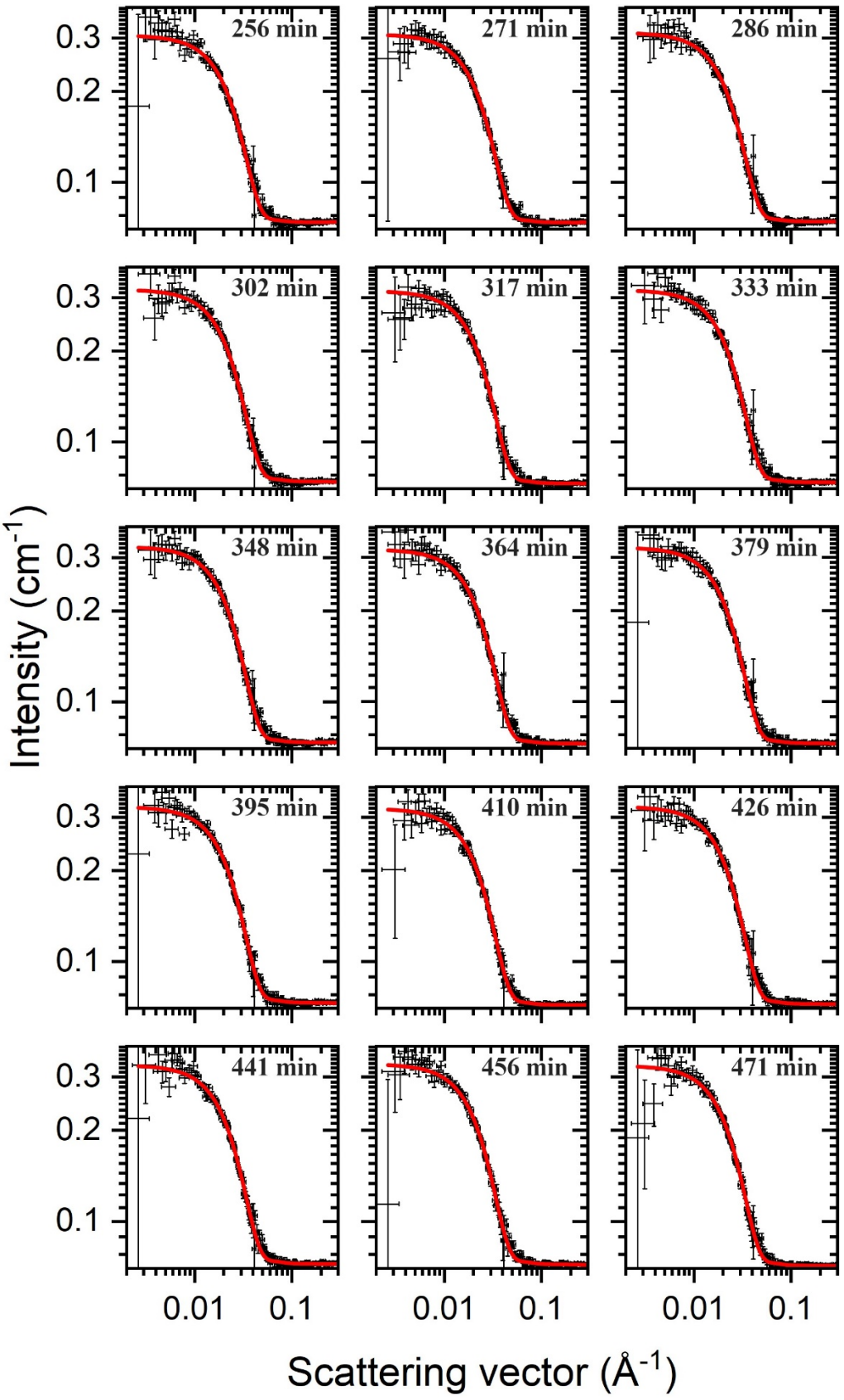

Figure S11. Time-resolved SANS monitoring of the dialysis self-assembly of G_{12}-*b*-Dex_{51} in presence of Ba^{2+}. Data were fitted using sphere form factor (red line).

Table S3. Parameters used to fit the SANS curves of the dialysis self-assembly of G_{12}-*b*-Dex_{51} in presence of Ba^{2+}. A monodisperse sphere form factor was used.

Time (min)	Scale (imposed)	Background (imposed)	SLD (10^{-6} Å^{-2})	SLD error (10^{-6} Å^{-2})	Solvent SLD (10^{-6} Å^{-2})	Radius (nm)	Radius SD (nm)
3	0.005	0.0753	6.253	0.020	6.4	5.61	1.12
24		0.0802	6.227	0.036		3.79	0.76
40		0.0787	6.292	0.013		7.38	1.48
55		0.0783	6.245	0.034		4.24	0.85
71		0.0777	6.232	0.023		4.93	0.99
86		0.0780	6.213	0.011		6.36	1.27
101		0.0774	6.111	0.008		6.14	1.23
117		0.0762	6.039	0.007		6.10	1.22
132		0.0757	6.000	0.006		6.36	1.27
148		0.0757	5.961	0.005		6.47	1.29
163		0.0759	5.939	0.004		6.55	1.31
179		0.0760	5.931	0.004		6.66	1.33
194		0.0746	5.917	0.004		6.59	1.32
209		0.0752	5.905	0.004		6.62	1.32
225		0.0744	5.905	0.004		6.66	1.33
240		0.0739	5.906	0.004		6.67	1.33
256		0.0738	5.900	0.004		6.70	1.34
271		0.0736	5.907	0.004		6.79	1.36
286		0.0742	5.903	0.004		6.78	1.36
302		0.0740	5.896	0.004		6.78	1.36
317		0.0729	5.897	0.004		6.77	1.35
333		0.0735	5.888	0.004		6.71	1.34
348		0.0733	5.898	0.004		6.87	1.37
364		0.0727	5.896	0.004		6.79	1.36
379		0.0728	5.905	0.004		6.92	1.38
395		0.0731	5.897	0.004		6.86	1.37
410		0.0719	5.899	0.004		6.85	1.37
426		0.0724	5.902	0.004		6.91	1.38
441		0.0724	5.893	0.004		6.86	1.37
456		0.0722	5.894	0.004		6.89	1.38

Table S4. SLD values of the components of the system

	density	SLD (x10^{-6} Å^{-2})
Ca	1.55	1.095
Sr	2.54	1.226
Ba	3.59	0.798
Na	0.971	0.923
H_2O	0.997	-0.559
D_2O	1.11	6.393
$C_6O_6H_5D_2$[a]	1.04	2.453

[a] guluronate units with hydroxyl protons exchanged with deuterium

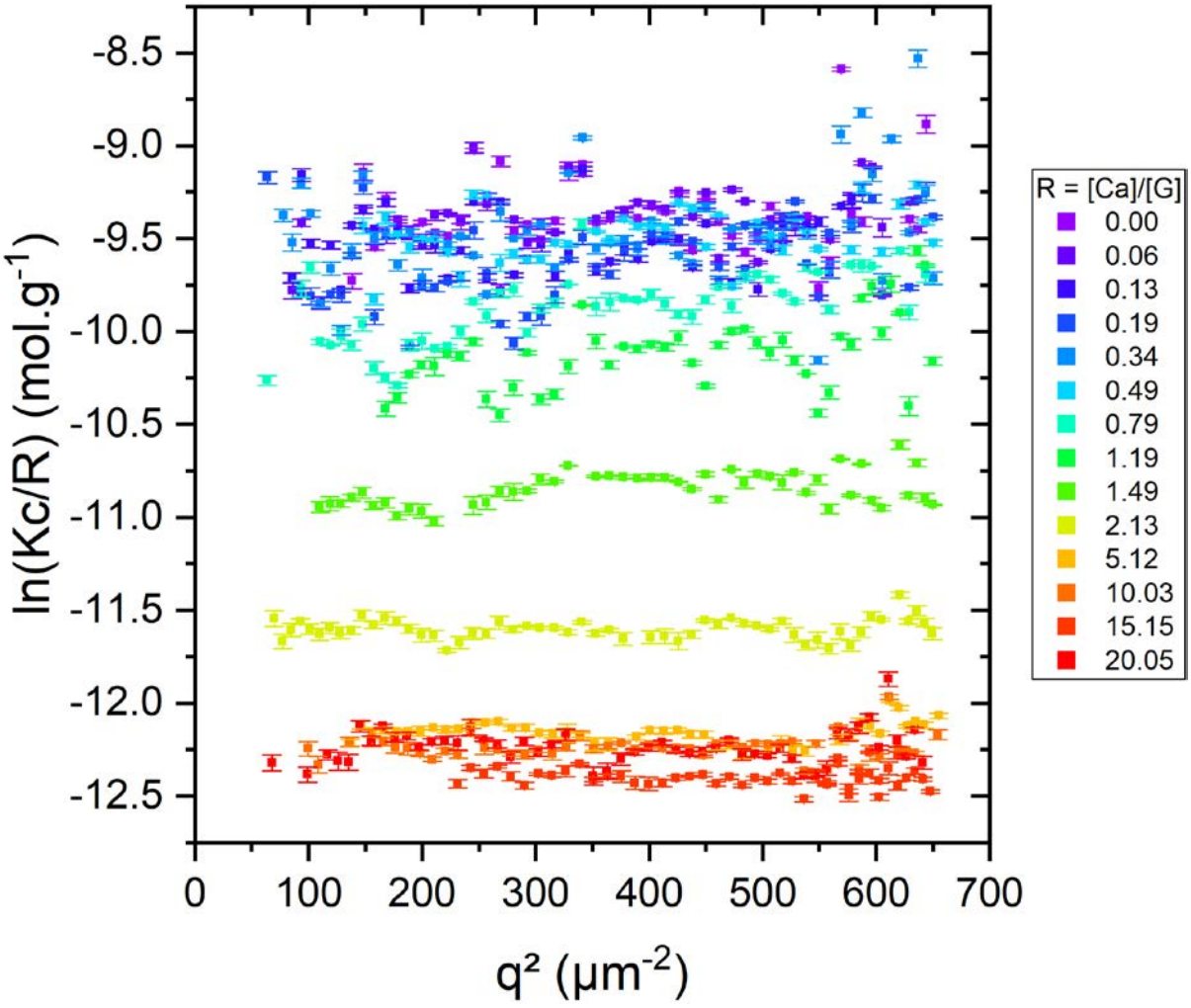

Figure S12. Static light scattering analysis of G_{12}-*b*-Dex_{51} solutions at 4 g.L^{-1} in 10 mM NaCl as function of R = [Ca^{2+}] / [G] following successive additions of 20 mM calcium chloride solution containing 10 mM NaCl. The Guinier-Zimm plots are plotted for each R value. The concentration c values take into account the dilution factor.

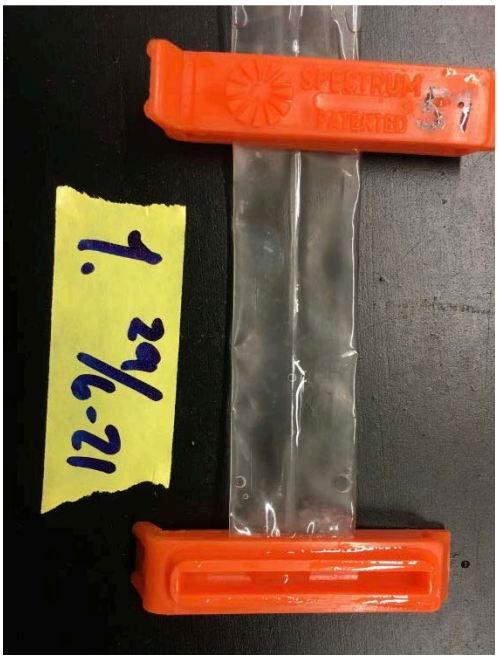

Figure S13. Precipitation of G_{28} upon dialysis against 20 mM$CaCl_2$ in 10 mM NaCl.

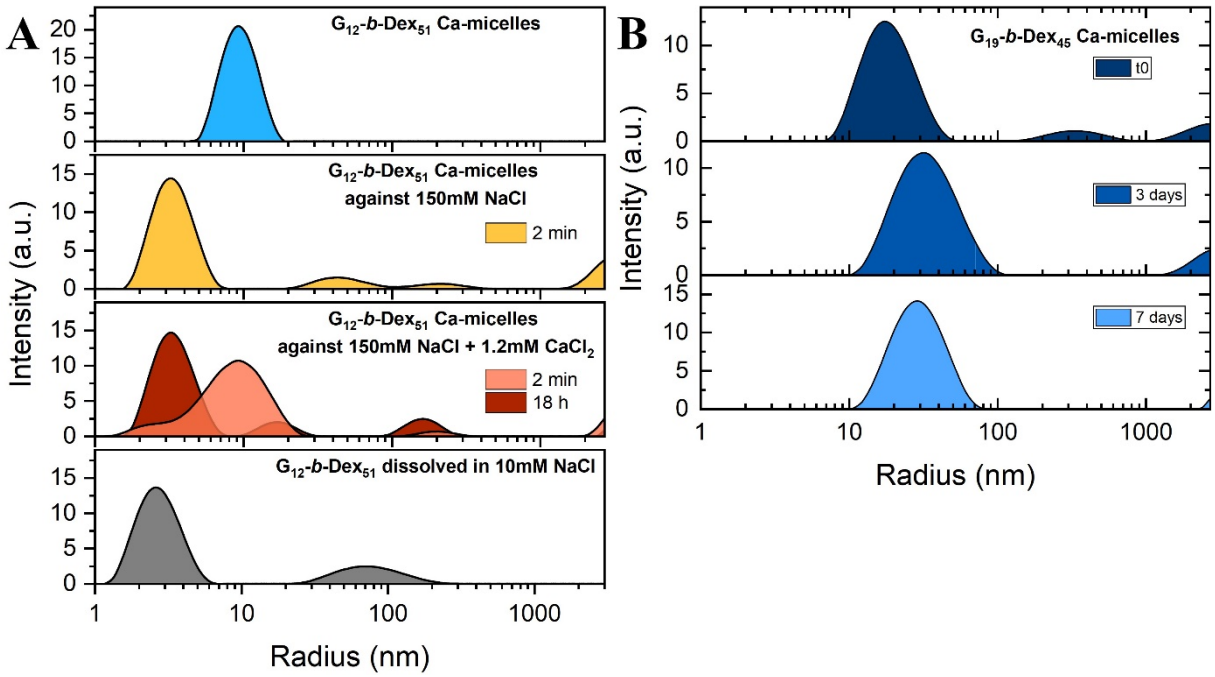

Figure S14. Stability of G_m-*b*-Dex_n micelles in saline conditions evaluated by DLS analysis. A) G_{12}-*b*-Dex_{51} micelles after dialysis against 20 mM $CaCl_2$ + 10 mM NaCl (top). The micellar suspension was then dialyzed against 150 mM NaCl or 150 mM NaCl + 1.2 mM $CaCl_2$. For comparison purposes, the size distribution of G_{12}-*b*-Dex_{51} dissolved in 10 mM NaCl is given (bottom). B) G_{19}-*b*-Dex_{45}/Ca^{2+} micelles upon dialysis against 150 mM NaCl + 1.2 mM $CaCl_2$.

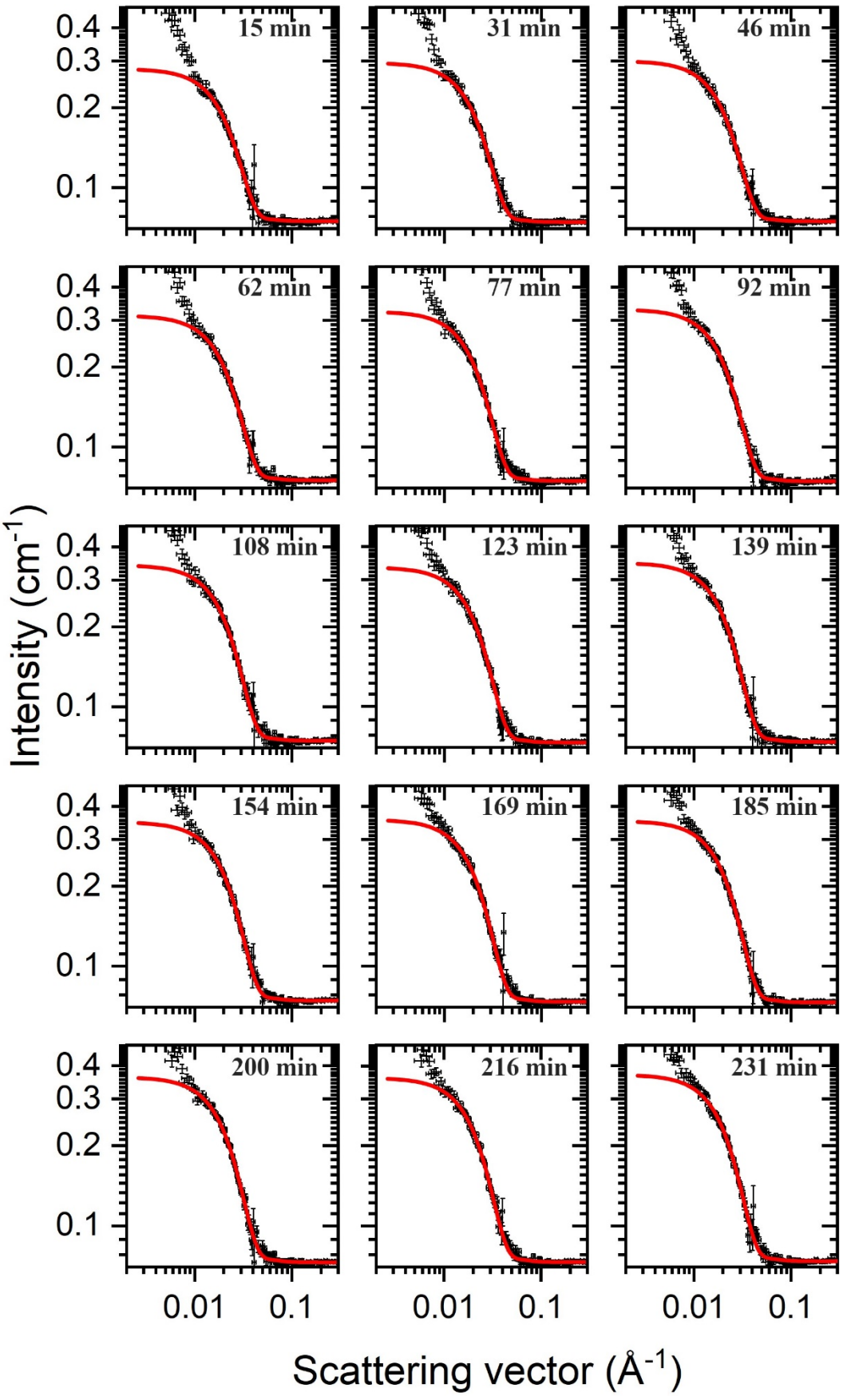
15 min
31 min
46 min
62 min
77 min
92 min
108 min
123 min
139 min
154 min
169 min
185 min
200 min
216 min
231 min
0.4
0.3
0.2
0.1
0.01
0.1
Intensity (cm^{-1})
Scattering vector (Å^{-1})

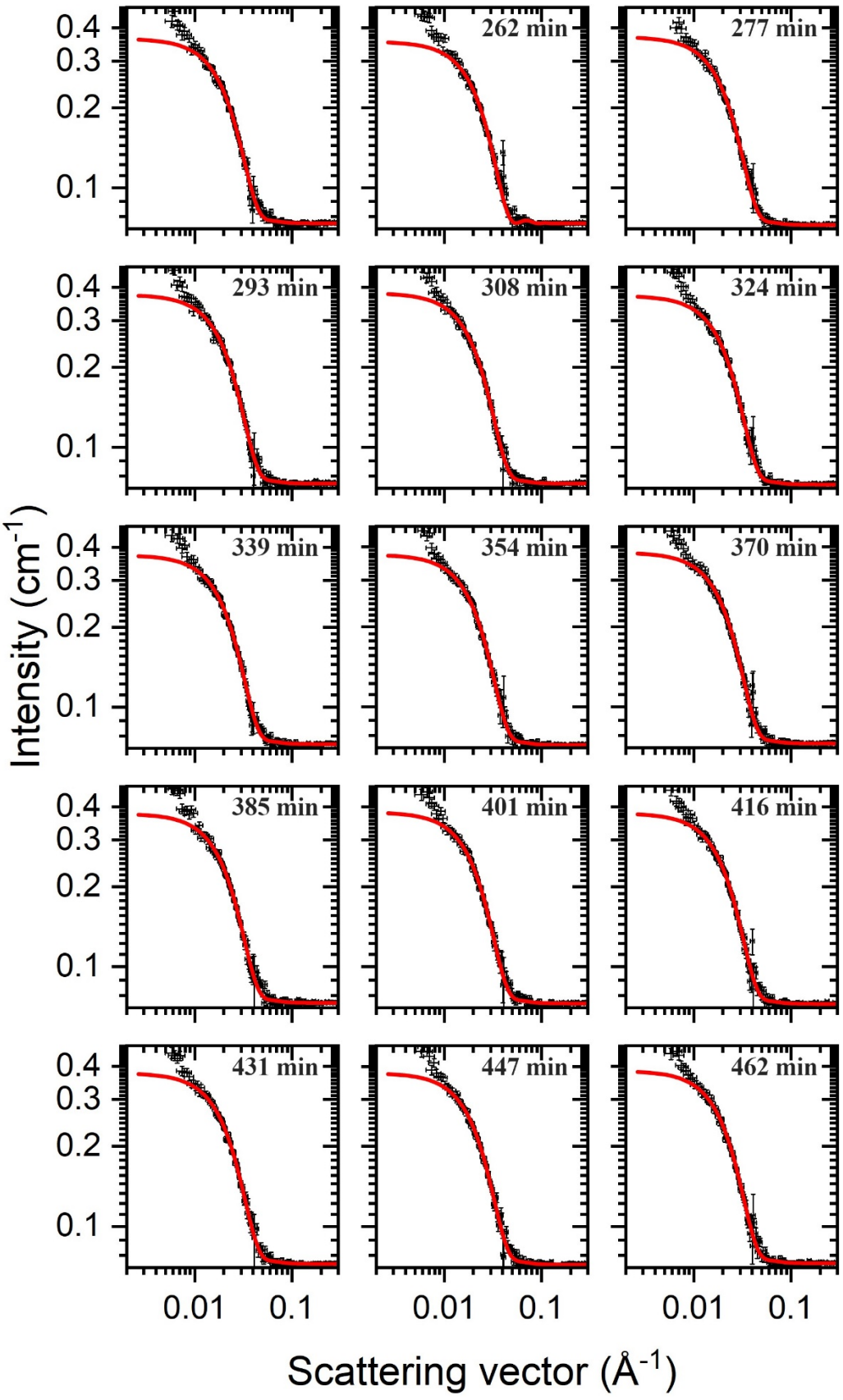

Figure S15. Time-resolved SANS monitoring of the barium ion exchange on preformed G_{12}-*b*-Dex_{51} nanoparticles by dialysis against calcium. Data were fitted using sphere form factor (red line).

Table S5. Parameters used to fit the SANS curves of the exchange dialysis for Ba^{2+} after self-assembly of G_{12}-*b*-Dex_{51} in presence of Ca^{2+}. A monodisperse sphere form factor was used.

Time (min)	Scale (imposed)	Background (imposed)	SLD (10^{-6} Å^{-2})	SLD error (10^{-6} Å^{-2})	Solvent SLD (10^{-6} Å^{-2})	Radius (nm)	Radius SD (nm)
0	0.005	0.075	5.991	0.004	6.4	7.36	1.47
15		0.074	5.977	0.003		7.37	1.47
31		0.075	5.972	0.003		7.36	1.47
46		0.075	5.957	0.003		7.32	1.46
62		0.075	5.950	0.003		7.36	1.47
77		0.074	5.948	0.003		7.40	1.48
92		0.074	5.935	0.003		7.36	1.47
108		0.073	5.935	0.003		7.31	1.46
123		0.074	5.926	0.003		7.34	1.47
139		0.074	5.915	0.003		7.23	1.45
154		0.073	5.920	0.003		7.36	1.47
169		0.073	5.914	0.003		7.26	1.45
185		0.073	5.910	0.003		7.32	1.46
200		0.073	5.904	0.003		7.23	1.45
216		0.074	5.906	0.003		7.33	1.47
231		0.074	5.901	0.003		7.23	1.45
247		0.073	5.892	0.003		7.18	1.44
262		0.073	5.897	0.003		7.25	1.45
277		0.073	5.894	0.003		7.26	1.45
293		0.073	5.890	0.003		7.26	1.45
308		0.072	5.889	0.003		7.19	1.44
324		0.072	5.891	0.003		7.21	1.44
339		0.072	5.890	0.003		7.22	1.44
354		0.073	5.892	0.003		7.29	1.46
370		0.073	5.897	0.003		7.30	1.46
385		0.073	5.894	0.003		7.31	1.46
401		0.072	5.896	0.003		7.30	1.46
416		0.072	5.883	0.003		7.17	1.43
431		0.072	5.889	0.003		7.23	1.45
447		0.073	5.888	0.003		7.28	1.46

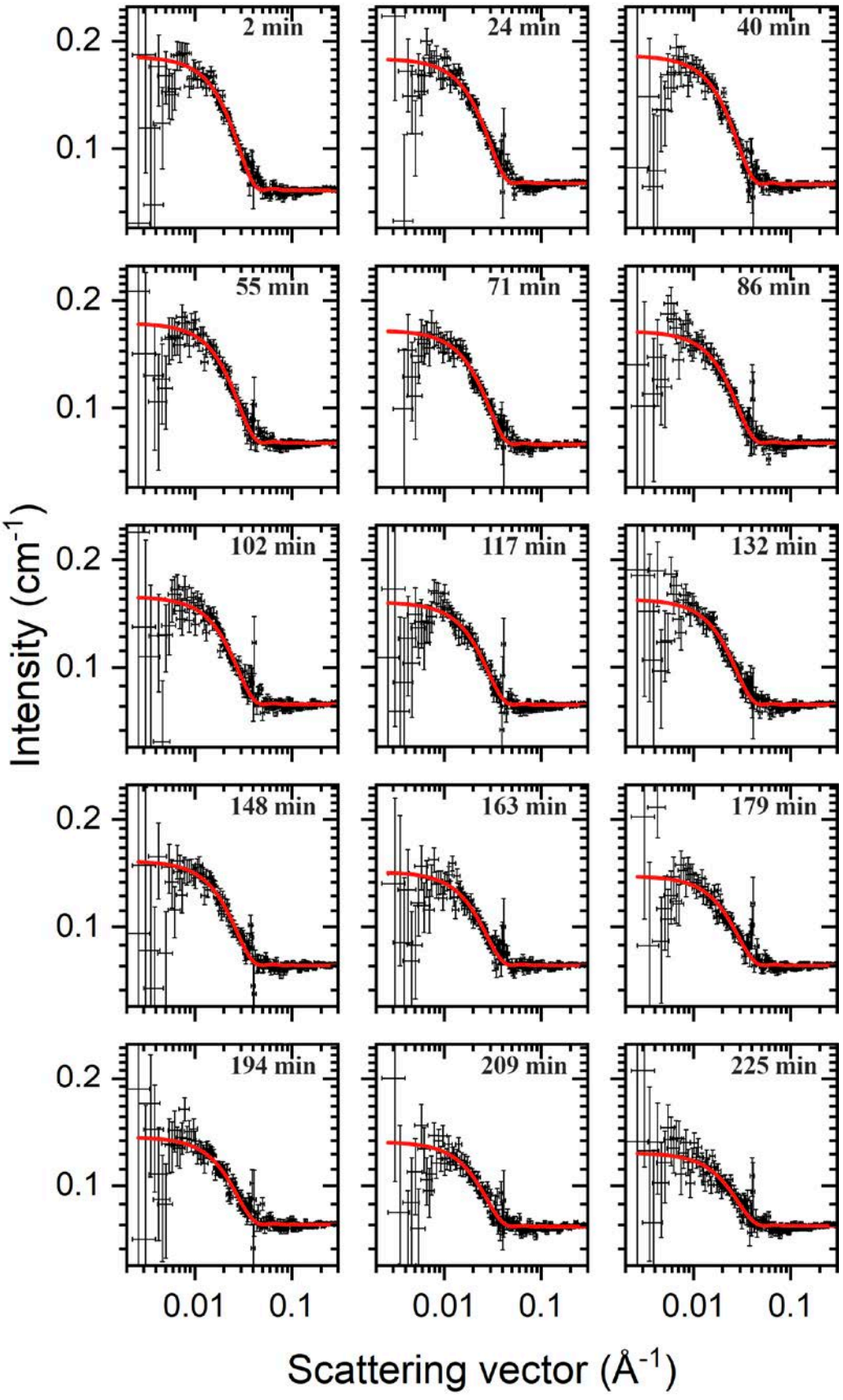
2 min
24 min
40 min
55 min
71 min
86 min
102 min
117 min
132 min
148 min
163 min
179 min
194 min
209 min
225 min
0.2
0.1
0.01
0.1
Intensity (cm^{-1})
Scattering vector (Å^{-1})

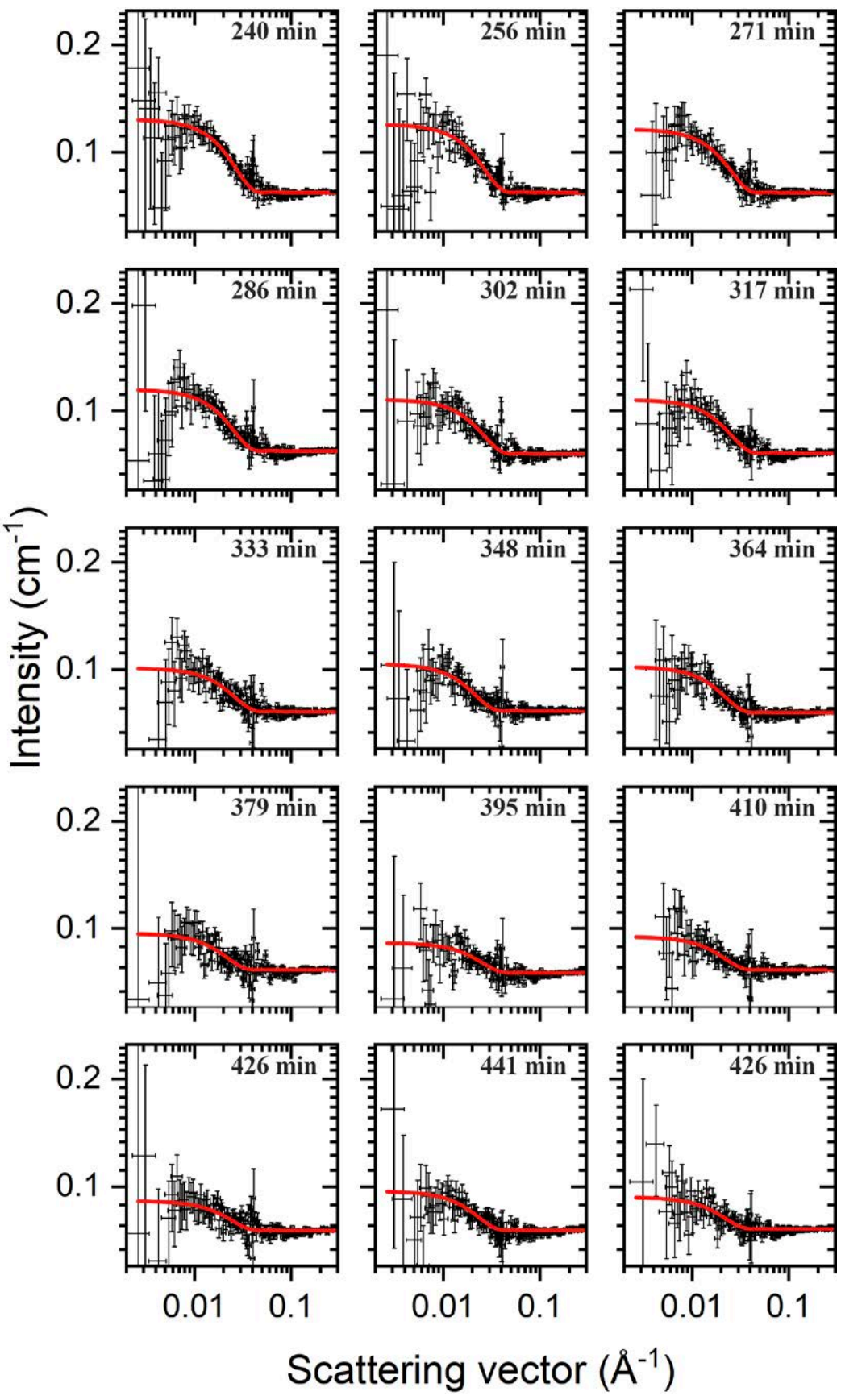

Figure S16 Time-resolved SANS monitoring of the EDTA exchange on preformed G_{12}-*b*-Dex_{51} nanoparticles by dialysis against calcium. Data were fitted using sphere form factor (red line).

Table S6. Parameters used to fit the SANS curves of the exchange dialysis for EDTA after self-assembly of G_{12}-*b*-Dex_{51} in presence of Ca^{2+}. A monodisperse sphere form factor was used.

Time (min)	Scale (imposed)	Background (imposed)	SLD (10^{-6} Å^{-2})	SLD error (10^{-6} Å^{-2})	Solvent SLD (10^{-6} Å^{-2})	Radius (nm)	Radius SD (nm)
3	0.005	0.0765	6.0054	0.0042	6.4	7.58	1.52
24		0.0800	5.9913	0.0047		7.28	1.46
40		0.0795	6.0054	0.0044		7.50	1.50
55		0.0795	6.0244	0.0044		7.60	1.52
71		0.0798	6.0203	0.0046		7.48	1.50
86		0.0792	6.0221	0.0049		7.30	1.46
102		0.0798	6.0390	0.0047		7.55	1.51
117		0.0788	6.0564	0.0048		7.59	1.52
132		0.0785	6.0602	0.0050		7.50	1.50
148		0.0786	6.0681	0.0047		7.70	1.54
163		0.0781	6.0745	0.0049		7.66	1.53
179		0.0782	6.0951	0.0052		7.66	1.53
194		0.0781	6.0743	0.0059		7.19	1.44
209		0.0781	6.1008	0.0054		7.57	1.51
225		0.0770	6.1070	0.0059		7.42	1.48
240		0.0774	6.1146	0.0066		7.21	1.44
256		0.0771	6.1348	0.0062		7.52	1.50
271		0.0771	6.1421	0.0066		7.41	1.48
286		0.0770	6.1729	0.0061		7.93	1.59
302		0.0771	6.1766	0.0062		7.94	1.59
317		0.0759	6.1775	0.0077		7.36	1.47
333		0.0761	6.1904	0.0073		7.65	1.53
348		0.0763	6.2077	0.0078		7.68	1.54
364		0.0765	6.2471	0.0066		8.82	1.76
379		0.0757	6.2456	0.0063		8.93	1.79
395		0.0767	6.2655	0.0075		8.83	1.77
410		0.0752	6.2473	0.0105		7.47	1.49
426		0.0766	6.2720	0.0071		9.20	1.84
441		0.0755	6.2563	0.0096		7.87	1.57
456		0.0755	6.2457	0.0083		8.08	1.62

References

(1) Solberg, A.; Mo, I. V.; Aachmann, F. L.; Schatz, C.; Christensen, B. E. Alginate-Based Diblock Polymers: Preparation, Characterization and Ca-Induced Self-Assembly. *Polym. Chem.* **2021**, *12* (38), 5412–5425. https://doi.org/10.1039/D1PY00727K.

(2) Fauquignon, M.; Porcar, L.; Brûlet, A.; Le Meins, J.-F.; Sandre, O.; Chapel, J.-P.; Schmutz, M.; Schatz, C. In Situ Monitoring of Block Copolymer Self-Assembly via Solvent Exchange through Controlled Dialysis with Light and Neutron Scattering Detection. *ACS Macro Lett.* **2023**, 1272–1279. https://doi.org/10.1021/acsmacrolett.3c00286.